The background features a 3D wireframe model of a hand on the left side, rendered in a light purple and blue color. On the right side, there is a detailed 3D model of a prosthetic joint mechanism, showing various components like a ball joint, levers, and rollers, rendered in a light blue and purple color. The overall aesthetic is technical and scientific.

Master Thesis

DESIGN OF A JOINT LOCK
FOR PROSTHETIC FINGERS

Gert Jan Pieterse

Faculty of engineering technology
Laboratory of biomechanical engineering

Examination committee

Hans Rietman
Bart Peerdeman
Edsko Hekman
Sarthak Misra
Dannis Brouwer

Document number

BW-353

Foreword

The design of the mechanics of the hand prosthesis is not yet over. Based on the proof of concept of a joint lock in this hand, more development and testing of the joint will have to be done. This will then be followed by even more work to develop a complete and well working hand. I hope this report will be valuable for the person who will continue working on this important project and can thus be a part in making the MyoPro hand prosthesis a reality.

At the end of the assignment, I would like to thank the people who helped me during the process. Bart, Hans, Edsko, Sarthak and Dannis, thank you for all the time spent with me, all the advice, tips, reviews of reports and more. This assignment would have been way harder or impossible without your help.

Gert Jan Pieterse

Summary

English

In the MyoPro project, where the Roessingh Research and Development and the University of Twente work together, a new myoelectrical prosthetic hand is developed. Part of the mechanical design of the hand involves the actuation system to enable the grasping of objects. An underactuated mechanism is desired, which requires less bulky and heavy actuators and enables natural grasping patterns. To restrain movement between specific phalanges, joint locks will be included to improve the control of the grasping patterns. In this assignment the development of such a joint lock is described. Several locking concepts are reviewed and two functional models are tested. A gear wheel mechanism, consisting of a toothed pawl that can lock a toothed gear wheel, requires a high actuation force and is thus unpractical. A friction amplifying mechanism, consisting of a drum and two friction pawls, provides self-locking behavior and is capable of withstanding joint loads of 2 Nm with low actuation force. This mechanism is further developed into a design of a two-fingered prosthetic hand.

Nederlands

In het kader van het MyoPro project, waar het Roessingh Research and Development en de Universiteit Twente in samen werken, wordt een nieuwe myoelectrische hand prothese ontwikkeld. Een van de onderdelen van het mechanische ontwerp van de hand is het actuatiesysteem dat de mogelijkheid moet bieden om verscheidene handgrepen uit te voeren. Er wordt voor gekozen om dit een onder-geactueerd systeem te laten zijn, dat minder grote en zware actuatoren nodig heeft en natuurlijke handgrepen mogelijk maakt. Om beweging tussen vingerkootjes te beperken, en hiermee meer controle te krijgen over de grepen, zullen blokkeringen in gewrichten toegepast worden. In deze Master opdracht wordt de ontwikkeling van een dergelijke blokkering uitgebreid omschreven. Verschillende concepten worden onderzocht en twee functionele modellen worden getest. Een tandwielmechanisme dat gebruik maakt van een pal dat in een tandwiel kan aangrijpen en ze het tandwiel blokkeert, heeft een hoge actuatiekracht nodig en is daarmee onpraktisch. Een wrijvingsmechanisme dat gebruik maakt van een cilinder en twee wrijvingspallen, heeft de eigenschap dat het zichzelf blokkeert en kan hiermee een koppel op het gewricht houden van minimaal 2 Nm met minimale actuatiekracht. Dit mechanisme is verder ontworpen tot een tweevingerige hand prothese.

Table of contents

Foreword	1
Summary	3
English	3
Nederlands	3
Table of contents.....	5
1 Introduction.....	7
2 Requirements of the lock	9
2.1 Introduction.....	9
2.2 Relevant background information on the hand	9
2.3 Specifications of the lock.....	12
2.4 Conclusion	15
3 Different concepts.....	17
3.1 Introduction.....	17
3.2 Concept A: Gear wheel.....	17
3.3 Concept B: Friction amplifying mechanism	18
3.4 Concept C: Band brake	20
3.5 Concept D: Rotational wedge.....	21
3.6 Comparing concepts to the requirements	23
3.7 Concept selection for development of functional models.....	24
4 Detailed design of the functional models	25
4.1 Introduction.....	25
4.2 Functional models of the Gear wheel	25
4.3 Functional models of the Friction amplifying mechanism	29
4.4 Conclusion	35
5 Testing the functional models.....	37
5.1 Variables to be tested	37
5.2 Test setup	37
5.3 Gear wheel mechanism.....	39
5.4 Friction amplifying mechanism	40
5.5 Connecting the actuator and release spring to the FA 4 model	42
5.6 Testing conclusions.....	43

6	Future design.....	45
6.1	Description of the joint design	45
6.2	Extra features	46
6.3	Important design changes.....	46
6.4	Description of the 2-fingered hand design.....	47
7	Conclusion and recommendations.....	51
7.1	Conclusion	51
7.2	Further recommendations	52
	Appendix A: Analysis of phases during forming of grasp types	55
	Appendix B: Free body analysis of the finger	57
	Appendix C: Calculations for the concepts.....	61
	Concept A: Gear wheel.....	61
	Concept B: Friction amplifying mechanism.....	62
	Concept C: Band brake	64
	Concept D: Axial wedge.....	65
	Appendix D: Other concepts	69
	Appendix E: 3D printed plastic models	71
	Gear wheel mechanism.....	71
	Friction amplifying mechanism	71
	Appendix F: Calculations for the functional models	73
	FEM analysis for the gear wheel model	73
	FEM analysis for the friction amplifying mechanism	74
	Hertzian contact stresses between the drum and the push pawls of the friction amplifying mechanism	75
	Calculating the contact angle tolerances for the FA 1 and FA 2 models of the push pawls of the friction amplifying mechanism.....	76
	Appendix G: Calculations for the future design	79
	Forces through the drum	79
	Maximum shear stresses and safety factor for pawl shafts.....	79
	References.....	81

1 Introduction

It is found that many upper-extremity amputees with myoelectrical hand prostheses do not use these devices.^[1] The main reasons for this are a lack of functionality, limited selectivity in control, lack of natural control, shortage of sensory feedback and loss of functional muscle contraction possibilities.^[2] To overcome these issues, the Roessingh Research and Development and the University of Twente are working together in the MyoPro project to develop a new myoelectrical hand prosthesis, including a virtual reality training program. Part of the project is the new mechanical design of the fingers to which this assignment contributes.

From analyzing the issues that currently limit the use of these prostheses the desire arises to minimize the number of actuators in the hand and couple the motions of the fingers. This will result in lower mass and volume while underactuation also provides an uncomplicated natural closing of the hand around an object. However, joint locks that can be controlled independently are required in order to gain control over separate fingers and execute specific grasp types.^[3, 4] These locks are meant to fit inside the distal interphalangeal joint, the proximal interphalangeal joint or the metacarpophalangeal joint of any finger of the hand prosthesis, which are shown in figure. The main function of the locks will be preventing the joints to rotate. This assignment will be focused on the design and testing of a joint with an integrated lock.

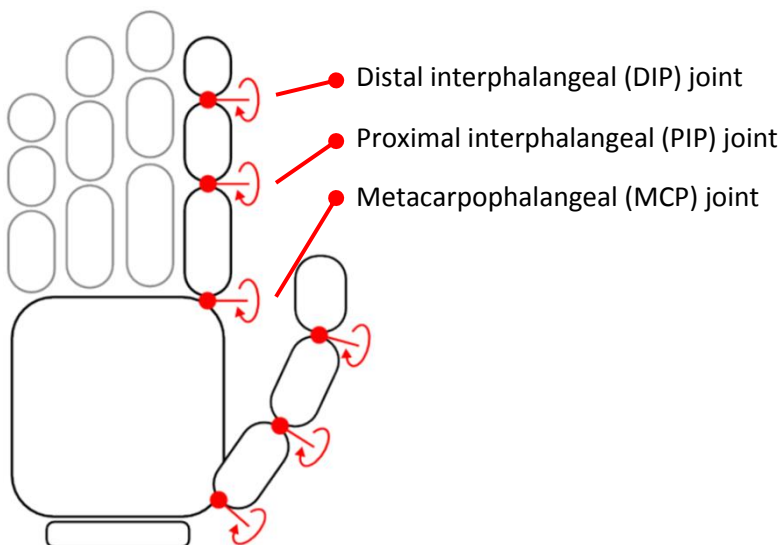


Figure 1: the important joint rotations where this lock can be placed: the distal and proximal interphalangeal (DIP and PIP) and metacarpophalangeal joints. For all these joints the lock will work for the flexion / extension movement only.

The objectives of this assignment have somehow changed during the process. At first, the main goal was to develop, build and test a 2-fingered hand, including underactuation and joint locks. After a while, it became clear that this goal was too high and the focus shifted to a thorough development of a joint lock. At the end of the assignment, it turned out that even a complete development of this lock required more time than what was available in this assignment. However, a working model was created and tested and thus a direction for the joint lock was set. Based on this model a future design for a 2-fingered model was made and several recommendations were done.

This report covers the relevant functions and requirements of the hand itself as well as the joint locks in chapter 2. Chapter 3 shows several lock concepts and a choice for the best promising concepts is made. The further development and detailed design of functional models of these concepts is explained in chapter 4. Chapter 5 deals with the testing setup and results. A future design for an improved joint lock and a 2-fingered model is shown in chapter 6. And finally the conclusion and further recommendations are described in chapter 7.

2 Requirements of the lock

2.1 Introduction

In this first chapter a foundation will be laid down for the design of the lock by looking at the requirements. To start with, some relevant background information of the total hand shall be used to understand the place of the lock in the total design. Further on, the grasp types that the hand should be able to perform will be analyzed to find the influence of locks in different joints in each grasp phase. With this information, the specifications for the locks will be set and calculated.

2.2 Relevant background information on the hand

Before it is possible to find the specifications for the lock itself, it is important to have a look at the complete hand the lock will be a part of. This background information is the framework for the design of the joint lock; where to implement it and what boundary conditions should be set. The metrics for the requirements follow from comparing to an average human hand or currently available myo-electrical handprotheses.

2.2.1 Underactuated mechanisms

It is assumed that the actuation system of the hand is a double underactuated mechanism which uses flexion tendons with differentials and extension springs. This means that the movement of one finger with respect to another finger is underactuated, but also that the movement of a particular phalange in a finger is underactuated with respect to another phalange in the very same finger. Several other hand prostheses, either currently available or for research purposes, use similar tendon-based underactuation.^[5-9] Figure 2 shows an example for a 2-fingered hand with such a system.

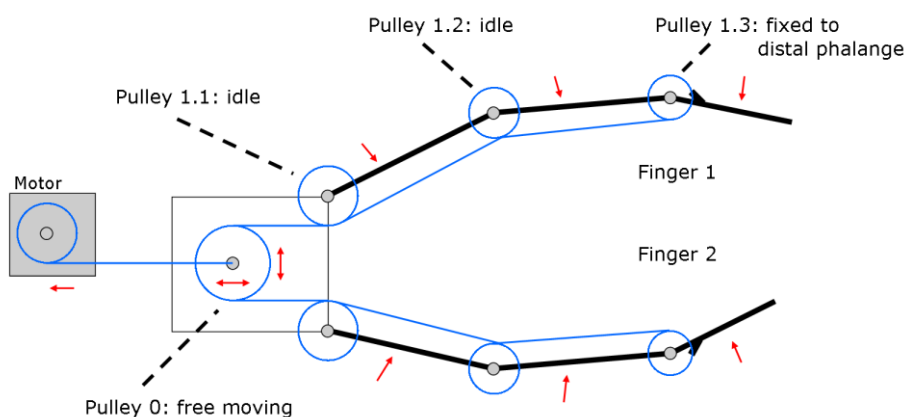


Figure 2: An underactuated 2-fingered hand. A tendon attached to the motor pulls the free moving pulley, located in the box. A second tendon is attached to pulley 1.3, runs over idle pulleys 1.2 and 1.1, over the free moving pulley 0, over idle pulleys 2.1 and 2.2 on finger 2 and is finally attached to pulley 2.3. When the free moving pulley 0 is pulled to the left, the fingers will have to bend but the shape of the movement of all phalanges depends on the friction in all joints and external loads on the phalanges. The free moving pulley 0 acts as a differential between the 2 fingers, and the idle pulleys 1.1 and 1.2 act as differentials within finger 1.

For a more complex 5-fingered hand, this means that a single actuator, being a DC motor, a pneumatic cylinder or any other type of small-sized actuator, drives the complete set of flexion tendons. These tendons are connected via differentials to each finger. A differential splits the motion but keeps the torque on all fingers equal. So when a finger touches a solid object, the movement of this finger will stop while the other fingers will continue their movement with increased velocity.

Analogue to the underactuation on finger-level, the underactuation on phalange-level also works with differentials. The MCP and PIP joint have idle pulleys on axes, which are acting as differentials. If one phalange touches an object and is prevented to move further, the other phalanges in the finger can still move on. The movement of the whole finger is dependent on the friction in the joints, loads on the phalanges, the radii of the pulleys and lengths of the phalanges.

When locks are implemented in the joints, it is possible to increase the control on the movement of all fingers and phalanges. Figure 3 shows the 2-fingered hand again, now with the joints in finger 2 locked. The free moving pulley 0, as being the differential between the fingers, now gives all motion to finger 1. The idle pulleys in finger 1, as the differentials inside this finger, distribute the motion to the phalanges. The shape of this movement again depends on the friction in the joints and loads on the phalanges. Finger 2 however will not move at all. If for instance, beginning with fully extended fingers, finger 2 would be locked completely and joints 1.2 and 1.3 of finger 1 as well, a very clear and well defined precision grasp can be obtained.

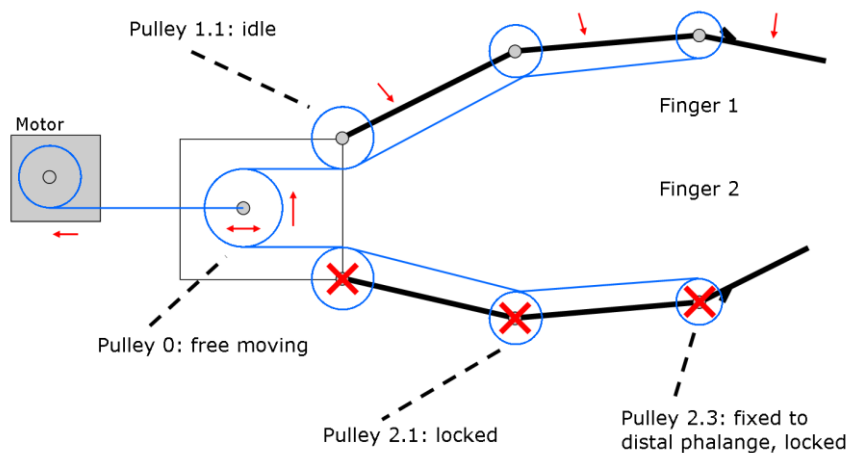


Figure 3: The same underactuated 2-fingered hand as before. Now with all the joints of finger 2 locked. Movement of the free moving pulley 0 to the left will cause finger 1 to bend. Again, the shape of the movement of the phalanges depend on the friction in the joints and external loads on the phalanges. Finger 2 will not move at all.

2.2.2 Functions of the hand

- 1) The hand is able to use 4 functional grasps or gestures: key grasp, cylindrical grasp, tripod grasp and finger point gesture. Figure 4 shows these grasps.
- 2) The flexion and extension of separate fingers and separate phalanges can be controlled.

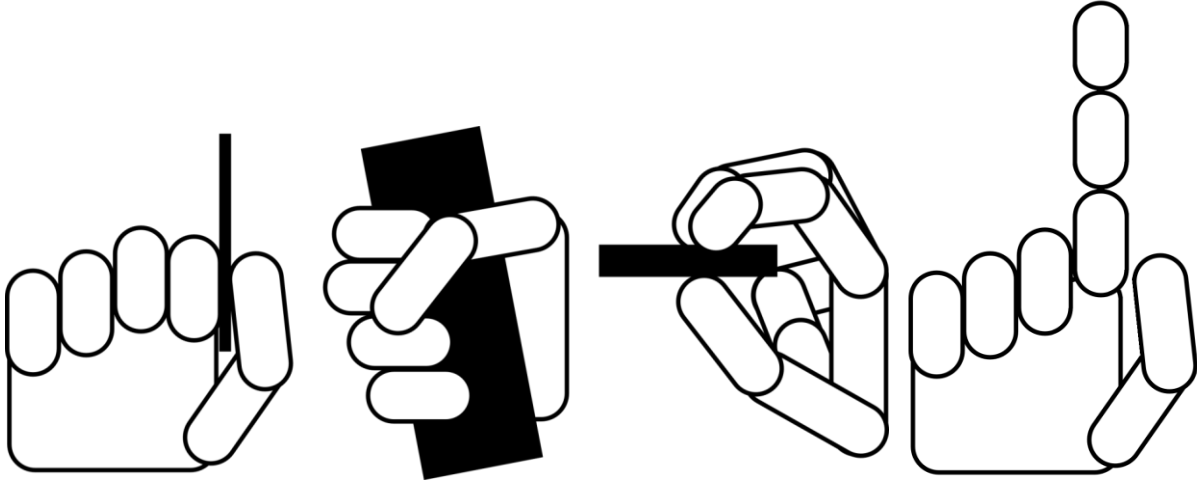


Figure 4: Functional grasp and gesture types: key grasp, cylindrical grasp, tripod grasp and finger point gesture.

2.2.3 Requirements of the hand

- 1) The hand is able to generate cylindrical and key grasp forces of 70 Newton and a tripod grasp force of 20 Newton.^[7, 10–13]*
- 2) Each finger contains 3 degrees of freedom for flexion and extension: in the DIP, PIP and MCP joints.
- 3) An underactuated differential system is able to actuate the flexion of finger joints.
- 4) Springs will allow the extension of the finger joints.
- 5) Total flexion of all fingers can be done within 1 second.^[2]
- 6) The range of motions for the flexion of the joints is from 0° to 90°.
- 7) For each joint the rotation can be measured.
- 8) The fingers have anthropomorphic dimensions.^[14]
- 9) The total weight of the hand is less than 500 grams.^[2]

* Note: the specifications for a tripod grasp in other hand prostheses vary from 5 to 20 N, whereas the single degree of freedom hands from Otto Bock can provide a 100 N grasp. Setting the requirement for the tripod grasp on 20 N is thus a high goal.

2.3 Specifications of the lock

2.3.1 Introduction

There are mainly 2 methods of locking the fingers. The first is to lock the pulley of the flexion tendon in the MCP joint so that the tendon has no means anymore to move the phalanges or put any loads on them. This however gives no control over separate phalanges and is thus disregarded. The other method is locking one phalange to the other one, so that complete control over the joint can be gained. The loads of the tendons will still act on the phalanges and multiple locks will be required in one finger. However, the number of locks per finger can be reduced by implementing a few passive joints, which means connecting phalanges across joints to each other so that 2 or 3 phalanges will move together. Choosing the number and locations of these passive joints can be decided later on and is part of the total design process of the complete hand.

2.3.2 Functions of the joint

- 1) Preventing motion between 2 phalanges.
- 2) Releasing the lock.
- 3) Measure rotational position.

2.3.3 Phases in the grasp types

To understand the consequences of the grasp types on the torques that the locks have to withstand, an analysis was made to understand different phases of all grasps. This analysis can be found in appendix A and a quick overview is shown in table 1. A cross through a joint means that the joint is locked, a line next to a phalange means that the phalange is in contact with an object and is thus exerting a load, grey phalanges mean movement of these phalanges.

Several different phases can be described, being either a locking phase or a movement phase. In these grasps, locking phases can be either without any loads acting on the phalanges or with loads on the fingertips. Movement phases can be with no loads at all, loads on the fingertips only or loads on all phalanges at the same time. To enable these grasps, the locks are mainly required to enable the locking phases for the different fingers.

Key grasp

<p><u>Locking</u> the thumb.</p>	<p><u>Moving</u> the index, middle, ring and little finger.</p>	<p><i>Unlocking</i> the thumb and <u>moving</u> the thumb until contact with the object.</p>

Tripod grasp

<p><u>Locking</u> the thumb, index and middle finger.</p>	<p><u>Moving</u> the ring and little finger to full flexion.</p>	<p><i>Unlocking</i> the index and middle finger, <u>moving</u> these fingers until contact with the object.</p>	<p><u>Locking</u> the index and middle finger while in contact with the object.</p>	<p><i>Unlocking</i> the thumb and <u>moving</u> the thumb until contact with the object.</p>

Cylindrical grasp

<p><u>Locking</u> the thumb.</p>	<p><u>Moving</u> the index, middle, ring and little finger until contact with the object.</p>	<p><i>Unlocking</i> the thumb and <u>moving</u> the thumb until contact with the object.</p>

Finger point

<p><u>Locking</u> the thumb and index finger.</p>	<p><u>Moving</u> the middle, ring and little finger to full flexion.</p>	<p><i>Unlocking</i> the thumb and <u>moving</u> the thumb until full flexion.</p>

Table 1: Different grasps and their phases. Cross: locked joints. Line next to a phalange: contact from this to the object and thus exerting a load. Grey: moving phalanges.

It is important to understand that the loads on the locks are a combination of the loads on the phalanges but also the load on the flexion tendon and the extension springs, located inside the fingers. Figure 5 shows how both the external force $F_{external}$ and the internal forces $F_{t,f}$ and $F_{t,e}$ have influence on the locking torque T_{lock} . The maximum loads on the fingers and in the tendons have to be calculated to be able to find the required locking torques in the joints.

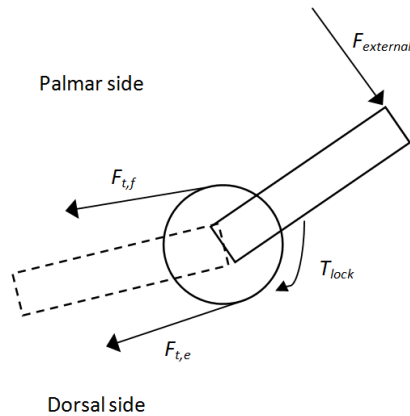


Figure 5: Sketch of the middle (left part) and distal phalange with a pulley connected to the distal phalange. An external force is shown on the tip of the finger and tendon or spring forces are shown on the flexion tendon (upper part of the pulley) and the extension spring. A locking torque acts on the joint between the 2 phalanges.

Analyzing the phases in table 1 where the locks are required, it shows that the locks are only useful in 3 specific phases: unloaded locking, locking with a load on the fingertips and movement with a load on the fingertips. These phases are thus examined in more detail below.

During all phases in the grasps where locking without any load is required, most of these phases are situations where no force is exerted on any of the other fingers, only movement of these 'free' fingers is required. This means that the locks involved only have small torques to withstand.

The phases where a fingertip load is exerted, either with locking or moving the finger, are only present in the tripod grasp. During phase 4 and 5, all joints of the index and middle finger need to be locked. Also during phase 5, with movement of the thumb, it would be favorable to lock the DIP and PIP joints of the thumb so that its shape remains under control. The specific requirements on the lock will thus follow from this particular situation. In appendix B, a free body analysis on all phalanges of a finger is done to calculate the maximum joint torques and forces. The tendon force is calculated to be 200 Newton at its maximum. The maximum joint torques that follow from these calculations are ± 2.0 Newton meter for the MCP joint, ± 1.2 Newton meter for the PIP joint and -1.2 to 0.6 Newton meter for the DIP joint. The maximum axial forces are 200 Newton and radial forces are 20 Newton on all joints.

2.3.4 Requirements of the lock

- 1) Withstand 2.0 Newton meter of torque, 200 Newton of axial force and 20 Newton of radial force.
- 2) A torque overload protection mechanism is included, which protects the important parts for torques above 6.0 Newton meter.
- 3) Locking is possible in both directions.
- 4) Locking and releasing can be done with a single actuator.
- 5) The lock should have an angular tolerance under 3°. *
- 6) Maximum dimensions are comparable with MCP joint dimensions: breadth (medial – lateral direction) 25 mm and depth (palmar – dorsal direction) 30 mm.^[14]
- 7) Favorable dimensions are comparable with PIP joint dimensions: breadth (medial – lateral direction) 18 mm and depth (palmar – dorsal direction) 17 mm.^[14]
- 8) The lock can be operated from -10° C to + 40° C.

* Note: It is not favorable that the lock has a large angular tolerance, since this can be demonstrated in a displacement of the fingertip. The fingertip may vary for 5 mm max as a result of angular tolerance in a single joint. For the MCP joint, this comes to a maximum angular tolerance of 3°.

2.4 Conclusion

In this chapter background information on the hand is analyzed and the required hand grasps are investigated. Along with other information this resulted in 3 functions and 8 requirements for the joint.

In the next chapter several concepts will be reviewed and compared with the requirements. Two concepts will then be chosen for further development.

3 Different concepts

3.1 Introduction

Four different concepts for the joint lock are considered in this chapter. For each concept the working principle is explained, basic calculations are made to find out the workability and potential restrictions on the use are investigated. Extra calculations are done in appendix C to achieve quantitative data. At the end of the chapter, each concept is compared to the requirements from the previous chapter and 2 concepts are selected for further development and testing.

Several other concepts are provided in appendix D but not worked out in more detail. All these concepts have significant short-comings when compared to the requirements in chapter 2.

3.2 Concept A: Gear wheel

The gear wheel concept consists of a radially toothed gear wheel with 2 toothed gear pawls at the sides, shown in figure 6. These gear pawls can rotate around shafts which give them the possibility to either lock or release the wheel. Actuation levers and release springs, as shown in the figure, are required to operate the concept. This concept is normally open, which means that the actuator will cause the lock to engage. A linear actuating mechanism will be required which will pull the lever away from the joint.

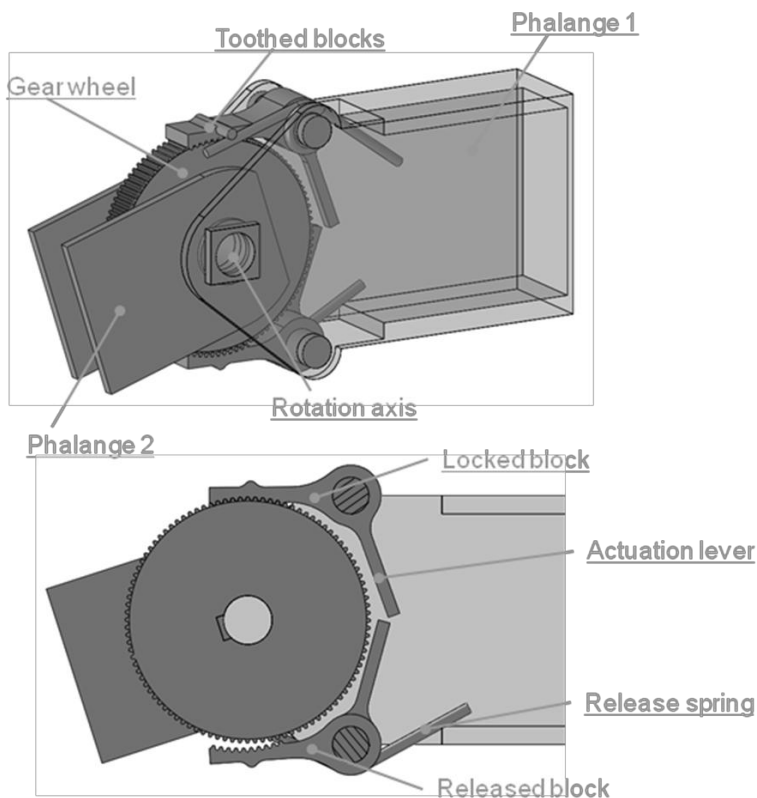


Figure 6: Gear wheel concept. Above: view of the concept with transparent Phalange 1 and axis. Below: side view with cross-section on the gear wheel with transparent Phalange 1 and axis.

A shortcoming of this concept is the rough indexing resolution, because with using a 20mm diameter gear wheel with module 0.2 and 100 teeth, the indexing resolution will be 3.6° . Finer gear wheel modules cannot be manufactured with conventional means. This also puts a lower limit on the size of the joint since a smaller gear wheel, with the same gear module, will automatically give an even rougher resolution. Also, if this concept is indeed self-locking, no overload protection mechanism is present, requiring a separate mechanism in the design. Another design difficulty might be the exact alignment of the gear wheel with the gear pawls.

3.3 Concept B: Friction amplifying mechanism

The friction amplifying mechanism concept is a rotational friction amplifying mechanism with a drum and friction pads on bars that rotate around another shaft, shown in figure 7.

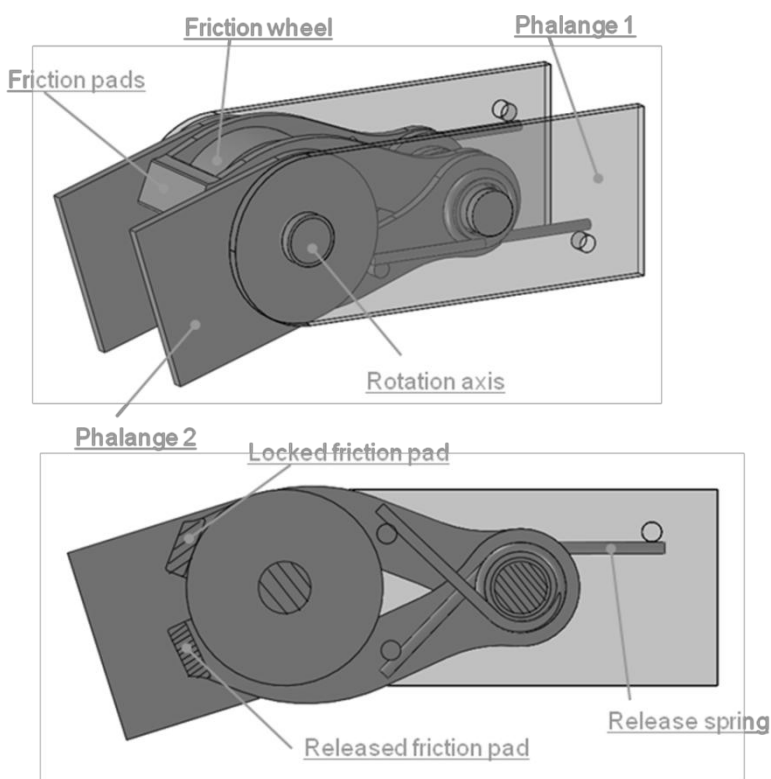


Figure 7: Friction amplifying mechanism concept. Above: view of the concept with transparent Phalange 1. Below: side view with cross-section on the wheel with transparent Phalange 1.

When a friction pad is pressed to the drum by a small start-up actuation force F_a , the friction from the rotating drum causes the bar to rotate further, increasing the normal force on the drum. Figure 8 shows these forces on the friction pad.

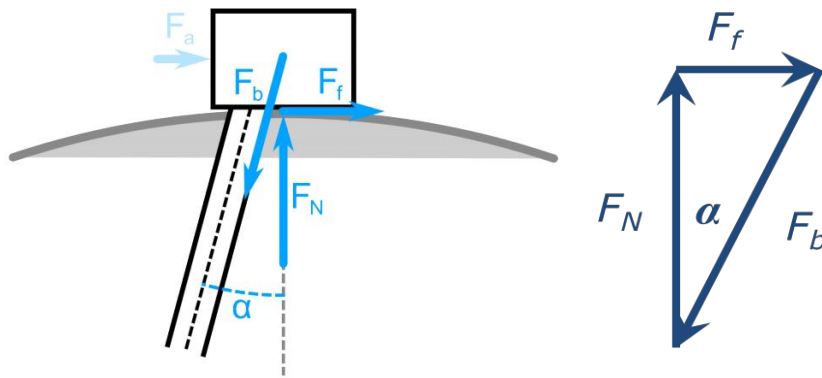


Figure 8: Sketch showing the force balance on the friction pad. The wheel rotates in clockwise direction and the actuation force F_a is only required as start-up.

If the angle α is below \tan^{-1} of the friction coefficient, self-locking will occur. In this case, the force through the bar F_b and the normal force F_n both increase such that the friction force F_f can theoretically increase infinitely. Therefore the locking torque, which is linear dependent on the friction force, also can increase infinitely. For releasing the lock, the external load on the lock has to be removed and the friction pad pulled from the wheel by a release force. For locking in both directions, 2 friction pads and bars are needed since the principle works unidirectional.

A potential drawback of this concept is the unknown release force. Theoretically, the release force can be very low when the external load is removed. But since tensions in the bars could possibly remain, there might be a risk of continued self-locking. If this occurs, a significantly higher release force is needed. This has to be verified by experiments with the functional models. For the functional model it can be useful to experiment with geometric variables since the exact geometry will influence the performance of the lock. Also, this concept has no torque overload protection mechanism.

3.4 Concept C: Band brake

The band brake concept works with a drum, connected to phalange 1, with bands or springs wound around it, as shown in figure 9. These bands are connected to phalange 2. In release mode, the bands are not touching the drum so the drum can rotate freely. In locking mode, the bands are tightened by actuators at their free ends, causing them to grip around the drum. Each band works best for locking a torque in one direction only.

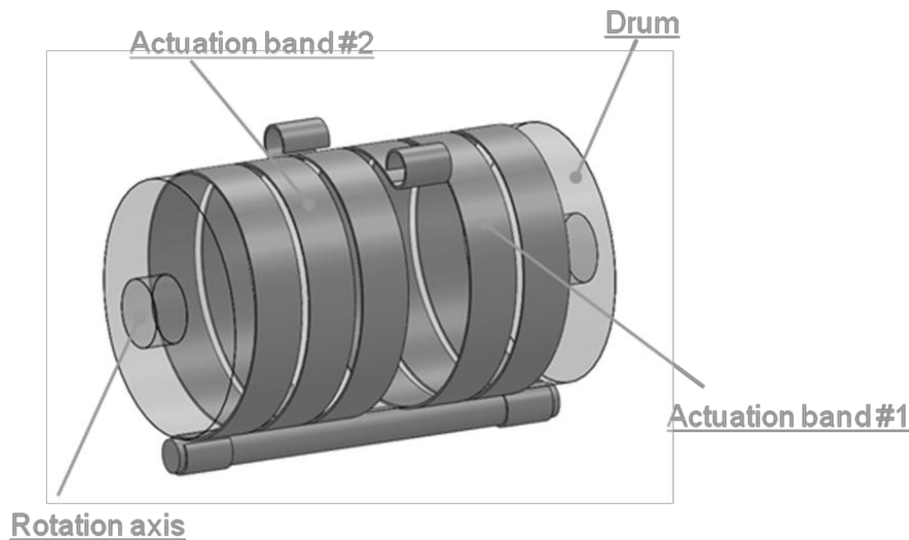


Figure 9: Band brake concept with transparent drum.

For this concept, several important requirements are unknown. The theoretical background of the band brake can be understood but the performance of the lock depends greatly on the precision of manufacturing and positioning of the parts. For instance, the locking torque can be calculated with the Capstan equation.^[15] While the simplified Capstan equation suggests that the locking torque with an acceptable actuation force will meet the requirements, it turns out that the bending stiffness of the band and non-linear frictional behavior between the band and the wheel have significant influence on the locking torque as well.^[16]

If in any case the band touches the drum on different parts of its helix before touching it completely, the principle of the lock is not met and the performance of the lock might be reduced significantly. Therefore the tolerances of the band will be tight. Due to the unknown exact working of the lock it is hard to estimate actuation and release forces so further research and testing would be required. The free movement friction also depends on the quality of manufacturing, since an occasional touch of the band to the drum might induce a lot of friction. Also, this mechanism has no overload protection mechanism included.

3.5 Concept D: Rotational wedge

The principle of the wedge is demonstrated for a translational situation in figure 10. Disc 1 is fastened at the top and has an inclined lower side. Disc 2 is flat and can move in 2 directions; translation in horizontal direction over a relatively long distance and a small displacement in vertical direction. A wedge with the inclined side matching disc 1 at the top and a flat bottom is located between the discs. This wedge can also move with small displacements in horizontal and vertical direction. In open position, the wedge will not touch either of the discs. In closed position, when the wedge does touch both discs, the friction coefficient between disc 1 and the wedge will be low and between disc 2 and the wedge the friction coefficient will be high.

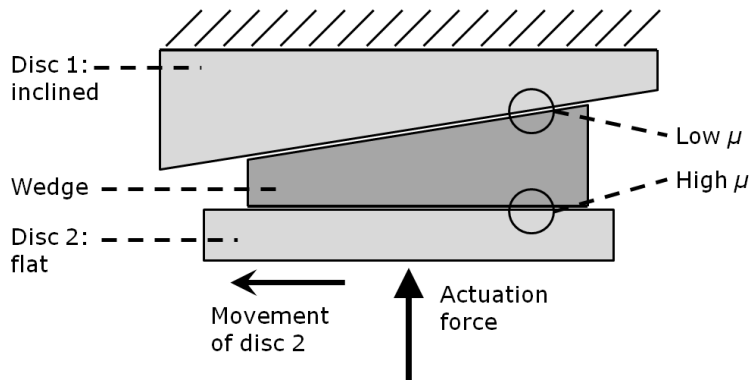


Figure 10: 2D sketch of the translational wedge principle.

When an actuation force is applied on disc 2, causing the disc to move up and pressing the wedge against disc 1, the closed position is achieved. When disc 2 moves to the left, due to the high friction with the wedge, it will drag the wedge along. Since the wedge has a low friction with disc 2, it can move but will soon be jammed in the gap because of the inclined side. If the lock is actuated non-backdriveable, a high normal force is thus induced which allows for a high friction force. The allowable friction force is depending on the angle of the curved sides and the low and high friction coefficients.

The rotational wedge concept has the same working principle as the translational wedge. It consists of a flat disc, connected to phalange 1, and curved discs, connected to phalange 2, as shown in figure 11. Rotational wedges of around 140 degrees are located between the discs.

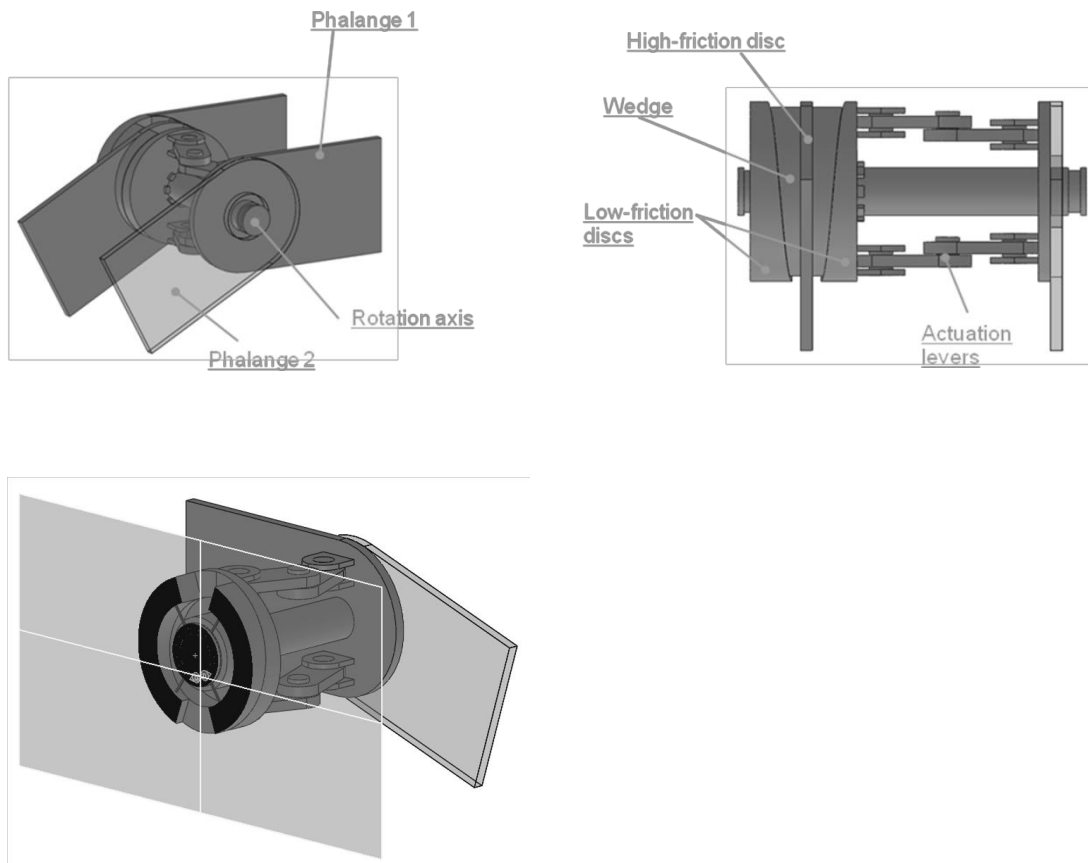


Figure 11: Wedge concept with partly transparent phalange 2. The figure below shows a cross-sectional view of the wedges, where the main shaft and rotational guidance mechanism for the wedges can be seen.

A major problem of this concept compared to the other concepts is its complexity. The wedges need a rotational guidance mechanism that bring the wedges back to their start positions but give them freedom to rotate with the flat disc. Also the manufacturing and positioning of components should be very precise to ensure alignment on the wedges and discs. Coatings are needed on one side of the wedges or on the curved discs to create low friction coefficients and have to be very resistant against wear. Furthermore, the mechanism should be kept clean since change in the friction coefficients due to dirty surfaces influence the lock performance.

As actuation mechanism a knee-lever could be used that can provide non-backdriveability. However, due to slipping at the beginning of locking a high normal tension force might remain in the mechanism after removing the external torque, requiring a high release force on the actuation mechanism.

3.6 Comparing concepts to the requirements

For each concept a brief explanation of the principle is given together with reasons for acceptance or rejection. Table 2 provides a list of requirements with ratings of importance and, if applicable, specifications for a comparison between the four concepts. The requirements are based on the requirements set in chapter 1 but also several general requirements are added.

	Impor- tance	Desired	Specifi- cations	Gear wheel	Friction ampl.	Band brake	Wedge
1) locking torque	***	High	2.0 Nm	√ *	√ *	? *	√ *
2) complexity	***	Low	...	√	√	-	X
3) number of actuators / actuation mechanisms	***	Low	...	√	√	√	√
4) actuation force / torque	***	Low	...	√ *	√ *	? *	√ *
5) actuation stroke	***	Short	...	√	√	-	√
6) release force / torque	***	Low	...	√	?	?	X *
7) joint movement for releasing	***	None	None	√	√	√	?
8) joint force	**	High	200 N	√	√	√	√
9) resolution for indexing	**	Fine	< 3°	X *	√	√	√
10) Dimensions (excl. actuator)	**	Small	25 x ∅ 30 mm	√	√	-	X
11) free-movement friction	*	Low	...	√	√	X	-
12) torque overload protection mechanism	*	Yes	Yes	X	X	X	X
13) involuntary joint movement at releasing	*	Low	< 3°	√	-	-	√
14) Operating temperatures	*	Wide	-10° to +40°	?	?	?	?

Table 2: Comparison of the concepts to the requirements. Meaning of symbols:

- √: requirement can be met
- : requirement cannot be met, small difference
- X: requirement cannot be met, large difference
- ?: meeting the requirement is unknown

* Note: follows from the calculations in appendix 3.

3.7 Concept selection for development of functional models

From the comparison of the concepts in paragraph 3.6, 2 concepts are selected for further development and testing. It is clear to see that the Gear wheel and Friction amplifying concepts meet most of the important requirements. The band brake concept is unclear about the possible locking torque as well as the required actuation and release force. The rotational wedge concept is too complex and requires a high release force. Therefore the gear wheel the friction amplifying concepts are chosen for further development.

In the next chapter these concepts will be designed in more detail and functional models for testing will be manufactured.

4 Detailed design of the functional models

4.1 Introduction

In chapter 3 a choice is made for 2 concepts to be developed and tested further: the gear wheel and friction amplifying mechanism concepts. Both will be discussed in more detail in this chapter, where the design of the functional models is explained as well as several variations on the design that are all tested. Where necessary, calculations are made to investigate the working of the models or the strength of the parts involved. Important design dilemmas are investigated and choices justified.

4.2 Functional models of the Gear wheel

4.2.1 Description

The SolidWorks model for the functional model with a single gear wheel lock is shown in figure 12. The model will have the possibility to act as both voluntary opening and voluntary closing mechanisms, since the locking cable pulls in horizontal direction. It is therefore easy to change the direction of the cable and use either a push-spring or pull-spring for releasing of the lock.

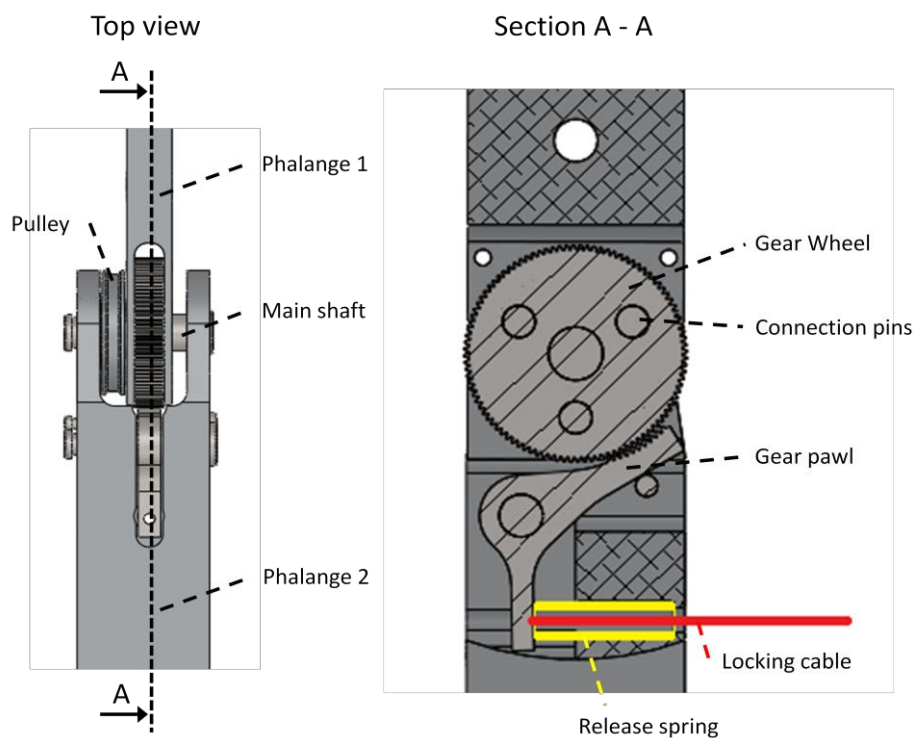


Figure 12: SolidWorks model for a gear wheel functional model. At the right a cross-sectional view is shown.

4.2.2 Important design choices

The most important modification compared to the concept in the previous chapter is the choice to use only 1 gear pawl for locking, as this makes the design much simpler and eliminates the over-constraining that would be introduced with 2 gear pawls. It also makes the design more compact since the gear pawl can now be placed inside phalange 1. A drawback is the fact that the locking torque will now result in a higher force from the gear wheel on the main shaft and its bearings, but with the chosen shaft diameter and bearings this should be no problem.

Another modification is the direct connection from the gear wheel to phalange 1 via 3 pins, pressed inside the holes in the gear wheel and phalange 1. This makes the design of the shaft and its connections simpler and stronger.

Different gear pawls will be made to test the optimal tooth shapes, as explained in paragraph 4.2.3. All gear pawls will be made from 3 mm thick machine steel and have a width at the teeth of 3 mm.

A FEM analysis in SolidWorks Simulation is done to find the maximum stresses in the gear pawl. The analysis is described in appendix E. The highest local stress on edges reaches 260 MPa. The general maximum stress is expected to be 160 MPa. Figure 13 shows the location of these stresses.

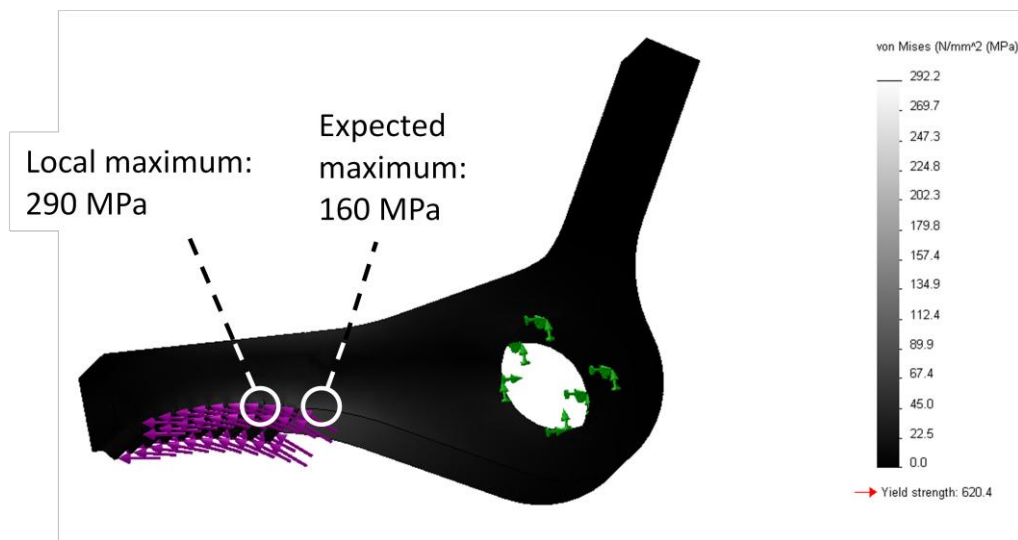


Figure 13: Von Mises stresses in the gear pawl at maximum load on the teeth. A FEM analysis using the SolidWorks Simulation tool.

Beside the gear wheel and the gear pawl, all the shafts will be made out of steel. The phalanges and pulley will have significantly lower loads on them, for which reason these parts will be made from aluminum which is easier to manufacture.

4.2.3 Variations on the design

- GW 1

The GW 1 model has a gear wheel of module 0.2 with 100 teeth. The gear pawl has 10 teeth with an intended involute tooth shape of 20° contact angle, as can be seen in figure 14. However, due to manufacturing mistakes the contact angle varies between 25° and 30° , as can be seen on the pictures taken with a SEM microscope and shown in figures 15 and 16. The gear wheel will be made with conventional gear manufacturing methods, including milling for making the teeth. The gear pawl will be made with wire-spark eroding in 1 phase, and the other parts mainly with milling and turning.

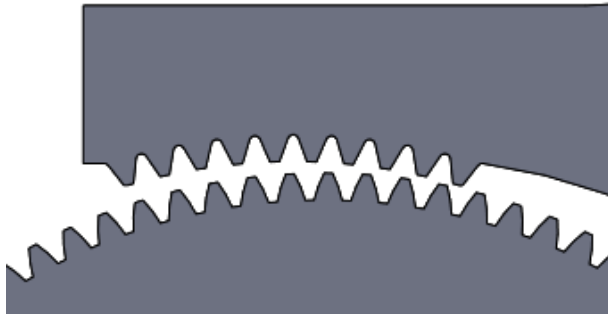


Figure 14: Detailed view of the gear pawl and gear wheel for the GW 1 model in SolidWorks.

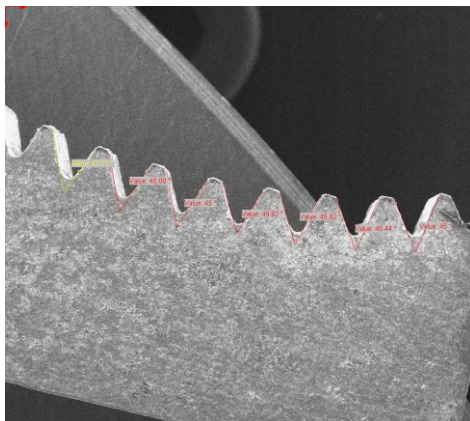


Figure 15: SEM picture from the GW 2 gear pawl, indicating that the contact angles are not consistent.

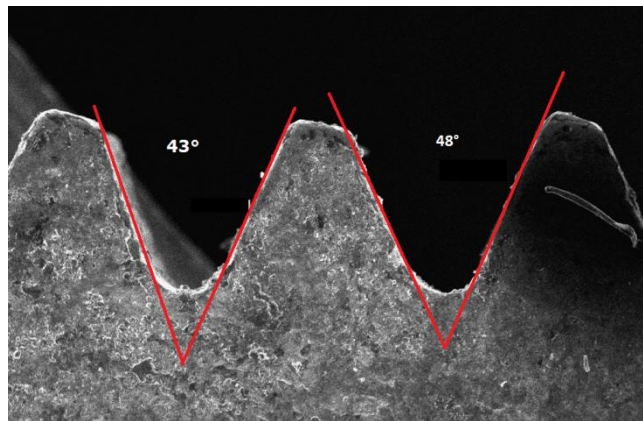


Figure 16: Zoomed SEM picture showing 3 teeth in detail, allowing the contact angles to be measured.

- GW 2

The GW 2 model uses the same gear wheel as the GW 1 model, but the tooth shape of the gear pawls is designed differently. The shape is intended with a sharp tip, as can be seen in the pictures from the SEM microscope in figures 17 and 18. The main reason for this design change is the idea that this shape might improve the ease of the teeth getting in contact with the gear wheel and thus improving the engaging of the lock. Manufacturing methods are the same as for the GW 1 model.

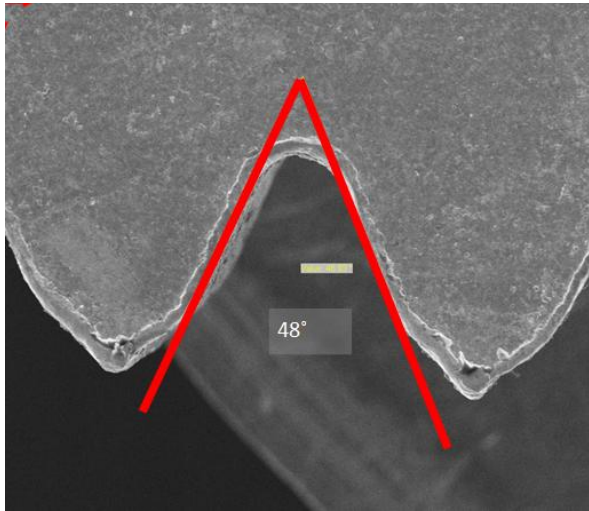


Figure 17: Zoomed SEM picture from the GW 2 gear pawl, showing the teeth in detail. The contact angle is measured and it is clear to see that the teeth are worn at the top.

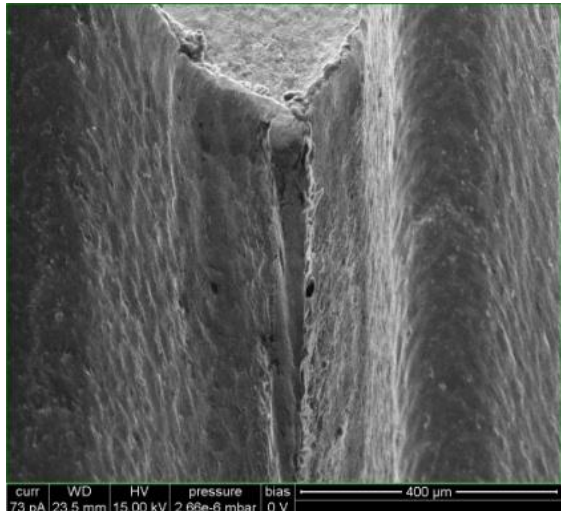


Figure 18: Zoomed SEM picture from another angle, showing the wear on the top of a tooth.

- GW 3

The GW 3 model is designed based on the GW 1 model, but with more precise manufacturing so the contact angles are very close to the intended 20°. The wirespark eroding process has therefore been done in 3 phases. Beside this change, also only 2 teeth are located on the gear pawl. With 10 teeth, it is hard to know exactly where the gear pawl and gear wheel are in contact. Therefore calculations are hard to validate and the behavior of the lock becomes direction-dependent. With only 2 teeth, the exact contact point can be predicted better and the lock works very consistent in both directions.

- GW 4

The GW 4 model is a renewed design, working with both a new gear wheel and a new gear pawl. The gear wheel teeth module is 0.5, allowing 40 teeth on the wheel. However, the tooth shape is not evolvente but straight and has a 15° contact angle, as can be seen in figure 19. Also, the gear wheel and gear pawl are hardened resulting in a better wear resistance. Both the gear wheel and the gear pawls are made with precise wirespark eroding.

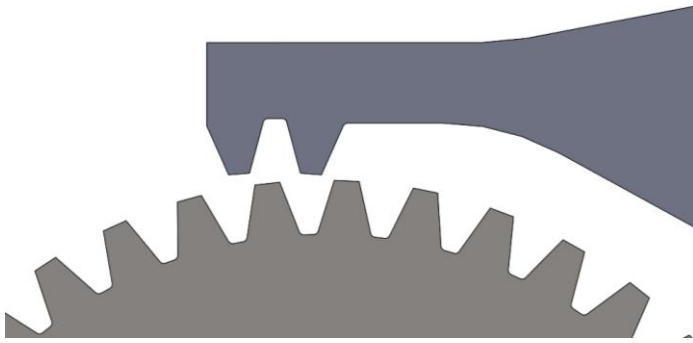


Figure 19: Detailed view of the gear pawl and gear wheel for the GW 4 model in SolidWorks.

4.3 Functional models of the Friction amplifying mechanism

4.3.1 Description

The SolidWorks model for the functional model with a double friction pawl lock is shown in figure 20. The mechanism has changed to push-pawl friction amplification instead of using the pull bars described in paragraph 3.3. The model will be a normally open mechanism, so the release of the lock will depend on the release spring. Probably fine-tuning of this release spring is required.

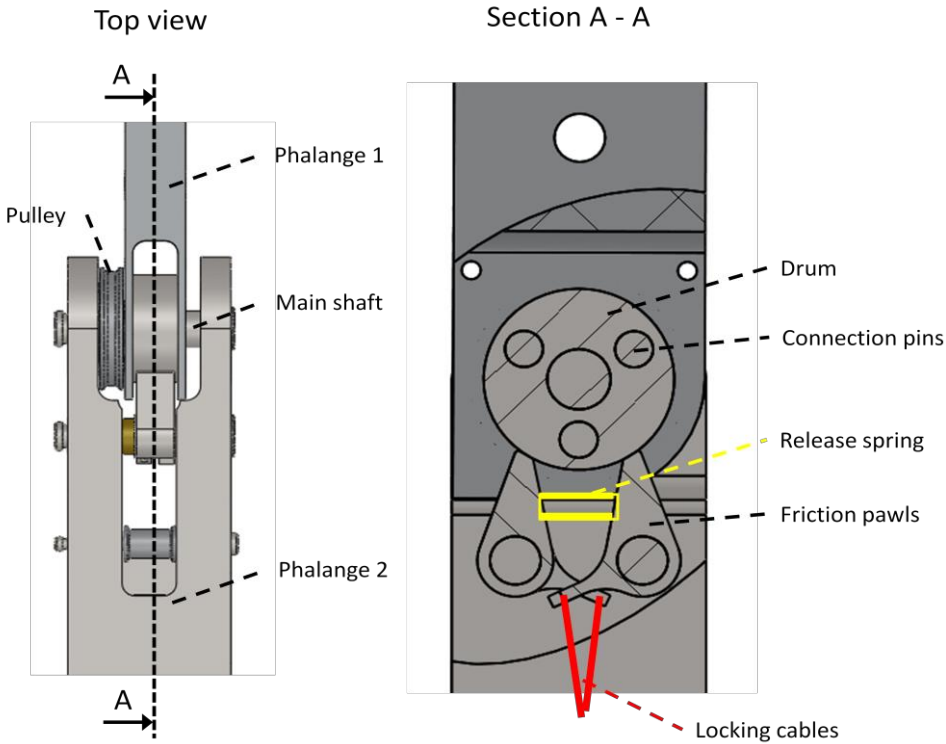


Figure 20: SolidWorks model of a friction amplifying mechanism functional model. At the right a broken out section of the side view is shown.

4.3.2 Important design choices

As noticed above, the most important modification is the use of push pawls instead of pull bars. Pull bars would not be strong and stiff enough to make the mechanism work and push pawls should work according to the same principle. Furthermore, the push pawls can be designed simpler and smaller.

Contrary to the pull bars, the push pawls will be mounted on separate shafts. With this, the pawls fit easier in the design and the mechanism can be made thinner.

Similar to the gear wheel model, the drum will be connected directly to phalange 2 with pins as this would make the mechanism stronger, simpler and thinner.

Since this concept works with the principle that the friction force causes the normal force to increase rapidly, the forces in the involved parts will be high. The most critical part will be the push pawls, where a FEM analysis is done to find the maximum stresses in the part. Appendix F shows the details on this analysis and figure 21 shows the stresses on the friction pawl from the FA 1 model. The highest stresses will reach 180 MPa, which is no problem for machine steel.

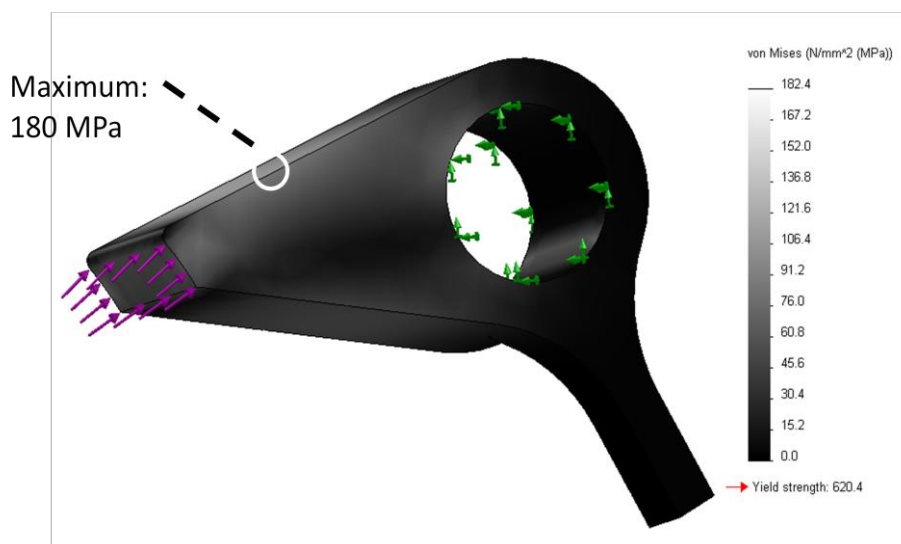


Figure 21: Von Mises stresses in the push pawl with a contact angle of 18° and at maximum load of 820 N. A FEM analysis using the SolidWorks Simulation tool.

However, the contact between the drum and the friction pawl will not be a well distributed stress contact implying the maximum stress at the contact area might be quite a bit higher. This can be calculated as the Hertzian contact stress and is done in appendix F. It results in a maximum contact stress of 900 MPa and an indentation depth of $1.8 \cdot 10^{-3}$ mm. If the friction pawls and drum are hardened, these stresses can be withstood. The drum must be harder than the friction pawls, so that the pawls will wear and the drum will remain round.

Several friction pawl geometries are designed providing different contact angles with the drum. For example the FA 1 model with a contact angle of 18° which should work with a friction coefficient of 0.3. The manufacturing tolerances for this geometry are calculated in appendix F as $\pm 3^\circ$ for the contact angle, which requires tolerances of maximum ± 0.03 mm for the important lengths like the

radius of the drum, the distance between the shafts through the drum and the push pawls and the length of the push pawls.

The material for the push pawls and drum should be steel which can be hardened for withstanding the contact stresses and extra wear resistance. The shafts have to with stand high loads and can be made from any steel alloy, depending on the availability in the workshop. Phalange 1 is important in the geometry of the mechanism and should be made out of steel as well, but phalange 2 and the pulley can be made from aluminum since high stiffness and strength is less important for these parts.

4.3.3 Variations on the design

- FA 1

The FA 1 model uses a drum with a 15 mm diameter and a push pawl with a contact angle of 18° . The contact area is flat. The pawl is 8.5 mm long and made with wirespark eroding. The other parts are made with milling and turning.

- FA 2

The FA 2 model is similar to the FA 1 model and uses the same drum, but is using a contact angle of 24° . This would require a higher friction coefficient but will also give a lower normal force.

- FA 3

The FA 3 model is made from the parts of the FA 1 model. The drum and push pawls are sand blasted for increased friction coefficient. The contact angle is reduced to between 6° and 10° to allow for an even lower friction coefficient. Figure 22 shows the parts after these modifications.

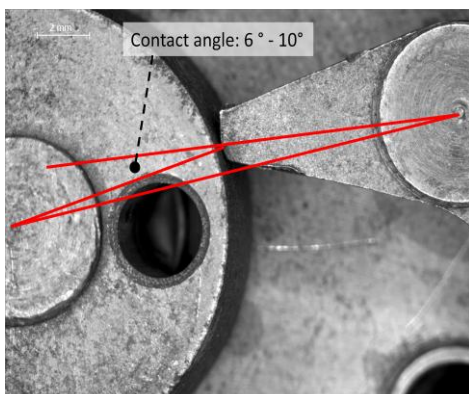


Figure 22: Microscopic picture of the FA 3 model with very low contact angle.

- FA 4 to FA 6

The FA 4 to FA 6 models are renewed designs, based on experiences with the FA 1 to FA 3 models. The drum is renewed but again with a 15 mm diameter and hardened. The push pawls are longer, 12.8 mm, which means that play in the mechanism will have less influence on the rotation of the pawls while engaged. The contact area is curved based on a logarithmic spiral. The advantage of such a contact area is that the contact angle with the drum will remain the same even when the pawl rotates slightly different than designed, which can be due to tolerances during manufacturing, play in the mechanism, wear of the parts or strain in the parts caused by the high loads. This will make the locking behavior of the lock more constant.

A logarithmic spiral is such a spiral, where the radius is dependent on the angle by:

$$r = a \cdot e^{b \cdot \theta}$$

where r is the radius, θ is the angle and a and b are constants of the spiral. Figure 23 shows such a spiral with the constants $a = 0.1$ and $b = 0.1$ with θ ranging from 0 and 100 radians.

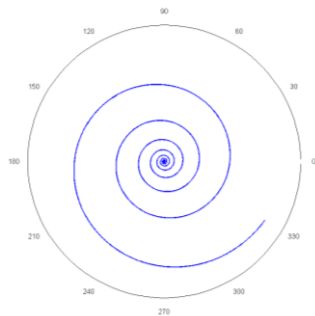


Figure 23: Logarithmic spiral with $a = 0.1$, $b = 0.1$ and $0 \text{ rad} < \theta < 100 \text{ rad}$.

A small part of this spiral is shown in figure 24 in blue, where also a circle with the same origin is displayed in red.

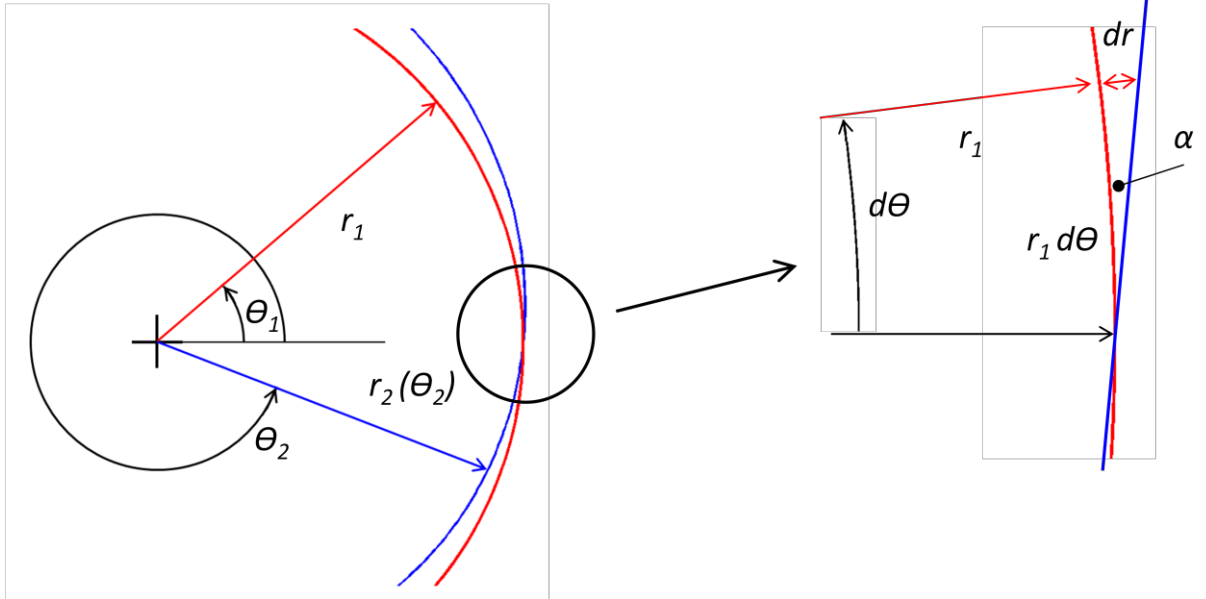


Figure 24: The intersection of a logarithmic spiral (in blue) with a circle (in red). The radius of the spiral, r_2 , is dependent on the angle θ_2 . The radius of the circle, r_1 , is constant. At the right a small section of the spiral is shown with an infinitesimal displacement of the angle $d\theta$.

As can be seen at the right part of figure 24, an infinitesimal displacement of the angle, $d\theta$, gives a change of the perimeter on the circle of $r_1 d\theta$, which by approximation is a straight line. However, the radius of the spiral increases with dr , creating the small triangle. The angle of the sharp corner, α , is thus:

$$\tan \alpha \approx \alpha = \frac{dr}{r_1 d\theta}$$

Since the growth of the radius can also be described as:

$$\frac{dr}{d\theta} = b \cdot a \cdot e^{b \cdot \theta} = b \cdot r$$

it follows that

$$\alpha = b$$

and is thus constant along the spiral. Using this property for the contact area of the friction pawl, figure 25 shows the contact area of the pawl in contact with the contact area of the drum. When the drum touches the spiral only in contact point C, the origin of the drum has to lie on the line BC perpendicular to the tangential line of the spiral. Therefore the angle between the line AC and BC is exactly α , and thus the contact angle of the mechanism. So, with choosing the constant b as the desired contact angle of the friction pawl, the profile of the contact area is determined.

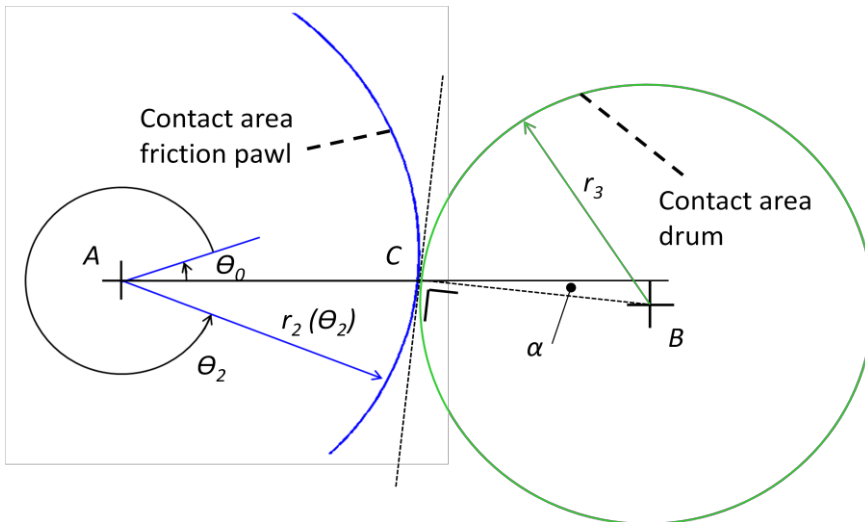


Figure 25: The contact area of the friction pawl as a logarithmic spiral with the radius r_2 depending on θ_2 . The whole pawl will also be rotated with θ_0 . The origin of the circle, indicating the contact area of the drum, will be on the line perpendicular to the tangential line of the spiral. Thus, the contact angle of the mechanism will be the same as the contact angle α of the spiral.

The friction pawl and drum for the FA 6 model are shown in figure 26. At the left, the nominal length between the shaft through the pawl and the drum is shown and it is clear that the contact angle is the desired 13° . At the right, the shaft is translated to the left with 0.9 mm, a distance much higher than the tolerance for the manufacturing of the parts. The pawl is rotated until in touch with the drum again, and this contact point is exactly the same as in the left figure, with the same contact angle of 13° . In a similar way, the tolerance in the radius of the drum does not affect the contact angle of the system.

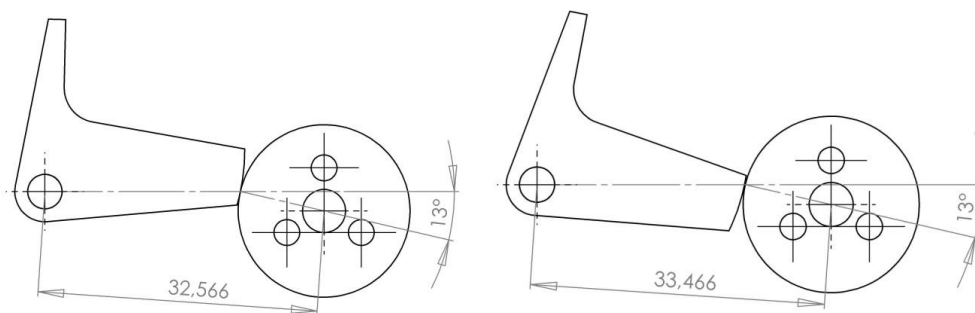


Figure 26: SolidWorks parts for the FA 6 model with 13° contact angle and logarithmic spiraled contact area.

The contact angle for the mechanisms are different for each model: the FA 4 model has a contact angle of 7° , the FA 5 model 10° and the FA 6 model 13° .

All push pawls are made from hardened steel to improve wear-resistance and withstand the high contact stresses.

4.4 Conclusion

In this chapter several functional models are designed, based on the chosen concepts of the gear wheel and the friction amplifying mechanism. The parts are partly manufactured by technicians at the university while other parts are ordered at companies in Twente. The next chapter will discuss the testing of these models.

5 Testing the functional models

5.1 Variables to be tested

With the functional models, several important variables of the lock were tested. The measurements will show whether the lock can achieve its required locking torque but will also determine the important requirements for the actuator. The following variables will be tested:

- 1) Investigate the self-locking behavior of the joint.
- 2) Measure the locking torque as a function of the actuation force if it is not self-locking.
- 3) Measure the actuation and release stroke of the gear and friction pawls.

After these tests, the most promising model should be combined with an actuator to test the total setup. From the results of the tests, an actuator has to be found with the right specifications and additional combined tests should be done:

- 4) Measure the required release force.
- 5) Investigate the working of the joint with actuator and release spring.

5.2 Test setup

The locks are located on a base plate, with the rotation axis in the vertical direction to have no influence of gravity on the testing. The phalange with the gear or friction pawl built in is connected directly to the base plate, leaving the phalange with the gear wheel or drum free to rotate. Figure 27 gives an overview of the setup where it is clear to see the lever connected to free moving phalange. At a distance of 200 and 300 mm from the rotation axis, holes are made in the lever to be able to connect a cable and force measurement spring to it. When the mechanism is locked it is possible to apply a tension force on the spring and thus introduce a measureable torque on the lock. Figure 28 provides a better detailed view of the pawl inside the fixed phalange and how this pawl can be actuated with a cable and force measurement spring. Before the first tests and between tests when necessary, the parts in contact were cleaned from any dirt and degreased.

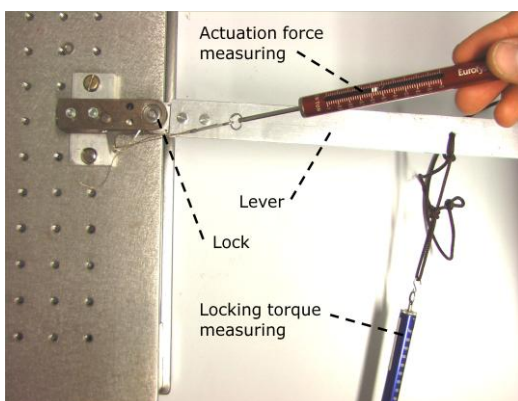


Figure 27: Overview of the setup with the force measurement spring for the actuation force (above) and the force measurement spring for the locking torque (right below).

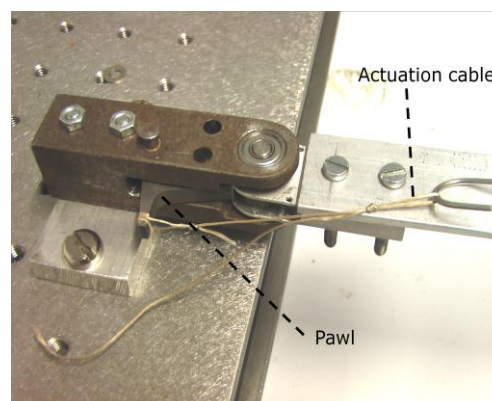


Figure 28: Detailed view of the lock including the cable connected to the pawl and the force measurement spring.

1) Investigating the self-locking behavior of the joint.

For this first test, the outcome will be that the lock is either self-locking or not. A lock will be regarded self-locking when, once engaged by a temporary actuation force, it will remain locked even after removing the actuation force or increasing the external locking torque. This is tested by actuating the lock with a small actuation force and once in its locking position, applying an external load on the lock. Next the actuation force is removed and it is observed whether the lock is able to withstand the load. To be considered functional, the lock must be able to withstand variations in the load, once locked.

2) Measuring the locking torque as a function of the actuation force if the lock is not self-locking.

For non self-locking mechanisms the actuation force can easily be measured by the force measuring spring connected to the lever of the gear or friction pawl. In the same way the locking torque can be measured by the force measuring spring connected to the lever on the free moving phalange.

An actuation force of 10 N in the actuation cable is applied. For the gear wheel concept, this will result in a contact point force of 13 N, and for the friction amplifying mechanism a contact point force of 50 N will be applied. The difference in contact point forces for both mechanisms is due to the different geometries of the gear and friction pawls.

For each mechanism, one model which seems promising but is not self-locking will be tested further to find the influence of varying the actuation force on the locking torque. If any difference of the locking torque due to the rotational orientation is found in the tests, this influence will be shown as well.

3) Measuring the actuation and release stroke of the gear and friction pawls.

Knowing the stroke of actuation that the gear and friction pawls have to make is important for selecting an actuator, since several linear actuator types have limited actuation strokes or stroke-dependent force outputs. The strokes can be found by measuring the rotation that the gear and friction pawl has to make from full releasing to full engagement.

4) Measuring the required release force.

The release force can be found when the cable attached to the gear or friction pawl is used in the other direction, and thus applying a force that is opposing the usual actuation force. The release force can then be measured with the force measuring spring.

- 5) Investigating the working of the joint with actuator and release spring.

When the variables of the chosen joint lock mechanism are known and an actuator with required specifications is found, theoretically the combined setup should work. Building this setup and testing whether the actuator combined with a release spring can indeed control the lock mechanism is a final check for the functionality of the design.

5.3 Gear wheel mechanism

5.3.1 Testing on all gear wheel models

The tests with the different variations of the gear wheel mechanism were done sequentially, where the results of the tests with the models GW 1 and GW 2 influenced the design changes for the models GW 3 and GW 4. The results of all the tests can be found in table 3. The actuation force of 13 N is the force exerted on the contact point, as is explained in paragraph 5.2. All tests were done twice, and the listed results are the averages.

Model names:

GW 1: teeth module 0.2, using a gear pawl with 10 evolvent teeth and 25° - 30° contact angles.

GW 2: teeth module 0.2, using a gear pawl with 10 sharp teeth and 25° - 30° contact angles.

GW 3: teeth module 0.2, using a gear pawl with 2 straight teeth and 20° contact angle.

GW 4: teeth module 0.5, using a gear pawl with 2 straight teeth and 15° contact angle.

Model:	GW 1	GW 2	GW 3	GW 4
1) Self-locking:	No	No	No	No
2) Locking torque with 13 N actuation force	0.4 Nm	1.0 Nm* _(CCW) 0.4 Nm* _(CW)	0.6 Nm	1.5 Nm
3) Actuation and release stroke:	0.8 mm	0.8 mm	0.7 mm	1.2 mm

Table 3: Test results for the gear wheel mechanism in all its variations.

* note: the maximum locking torque of the GW 2 model reduced quickly, due to wear of the teeth.

(CCW) means in counter clock-wise direction only.

(CW) means in clock-wise direction only.

5.3.2 Further testing on the GW 4 model

As can be seen in the table, none of the models is self-locking. The GW 4 model gives the best results with the highest consistent locking torque. For this model, a graph is given in figure 29 where the locking torque as function of the actuation force is measured.

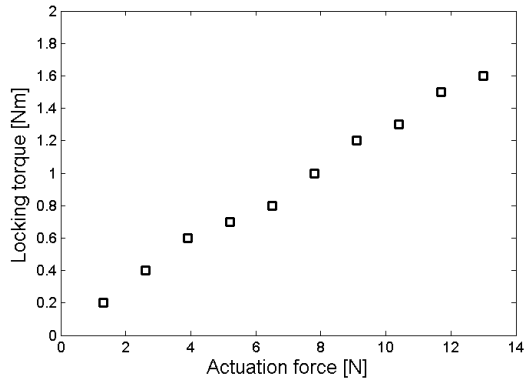


Figure 29: Locking torque as function of the actuation force for the GW 4 model.

5.4 Friction amplifying mechanism

5.4.1 Testing on all friction amplifying mechanism models

The tests were started with the models FA 1 and FA 2. The FA 1 model was then transformed to the FA 3 model, and later on the redesigned FA 4, FA 5 and FA 6 models were made. The results of the tests can be found in table 4. The actuation force on the point of contact is 50 N for this mechanism, as explained in paragraph 5.2.

Model names:

FA 1: 18° contact angle with flat contact area.

FA 2: 24° contact angle with flat contact area.

FA 3: 6° - 10° contact angles with increased surface roughness.

FA 4: 7° contact angle with spiraled contact area.

FA 5: 10° contact angle with spiraled contact area.

FA 6: 13° contact angle with spiraled contact area.

Model (<i>angle</i>):	FA 1 (18°)	FA 2 (24°)	FA 3 (6° - 10°)
1) Self-locking:	Yes *	No	Yes
2) Locking torque with 50 N actuation force	2.0 Nm *	~ 0 Nm	1.0 Nm **
3) Actuation and release stroke:	0.2 mm	0.2 mm	0.2 mm

Model (<i>angle</i>):	FA 4 (7°)	FA 5 (10°)	FA 6 (13°)
1) Self-locking:	Yes	No	No
2) Locking torque with 50 N actuation force	> 2.0 Nm	1.5 Nm	0.3 Nm
3) Actuation and release stroke:	0.2 mm	0.2 mm	0.2 mm

Table 4: Test results for the friction amplification mechanism in all its variations.

* Note: only during first test series, but very inconsistently.

** Note: Though self-locking, the torque was limited, since the friction pawl was forced beyond its locking position when the lock was loaded with more than 1.0 Nm locking torque.

5.4.2 Further testing on the FA 4 and FA 5 models

The FA 4 model is selected for further testing, including test 5 in combination with the actuator and release spring. Therefore, first test 4, testing the release force, is performed and gives the following result:

Release force for FA 4 model with 2.0 Nm load: 0.3 N.

When testing this FA 4 model, it showed that with higher locking torques the lock has quite some flexibility; with 1.0 Nm the drum does rotate 11°, and with 2.0 Nm a rotation of 15° occurs.

The FA 5 model is selected as the model with the highest locking torque but without self-locking and is thus tested in more detail. The behavior of this model appears to be dependent on the rotational orientation and therefore the locking torque is tested for 3 orientations to cover the range of the joint. One test is at full extension, so with an angle of 180° between the phalanges, one test with an angle of 135° and at almost full flexion, with an 95° angle. In figures 30 to 32 the graphs are given where the locking torque as function of the actuation force and rotational orientation is measured. At the measurements where the locking torque is given as 2.0 Nm self-locking occurred. The model was not loaded above 2.0 Nm because of risk of damage to the model.

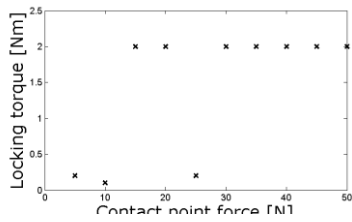


Figure 30: Torque as function of the actuation force for the FA 5 model, at full extension, so 180° angle.

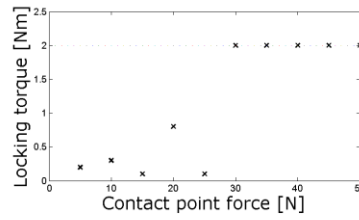


Figure 31: Torque as function of the actuation force for the FA 5 model, at 135° angle.

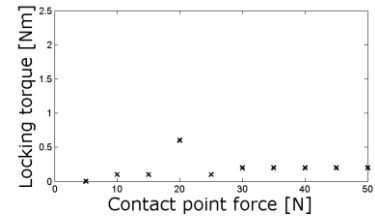


Figure 32: Torque as function of the actuation force for the FA 5 model, almost at full flexion, so 95° angle.

The plots for the 180° and 135° angles show that after a certain minimum actuation force, self-locking occurs. But for all plots, if there is no self-locking the locking torque is relatively low and mostly without dependence on the actuation force. Also, the self-locking is best at full extension and not present at flexion.

5.5 Connecting the actuator and release spring to the FA 4 model

Knowing that the FA 4 model is self-locking, the actuator only has to deliver a force large enough to overcome the release spring and move the pawl a little bit to touch the drum. Figures 33 and 34 show the setup with actuator and release spring. A 110C 6V solenoid, the smallest available, is used. Fine-tuning was required to set the actuator on its place and obtain the required release spring stiffness. The setup then worked well.

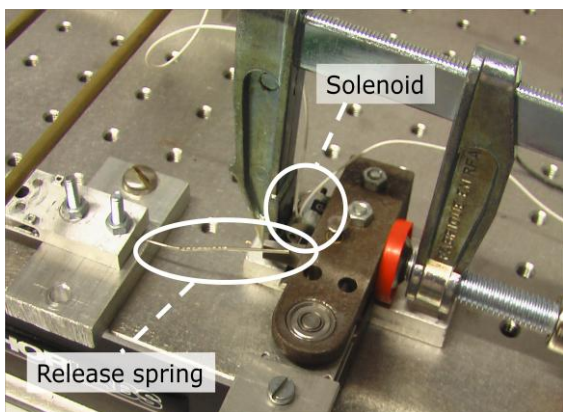


Figure 33: Detailed view of the FA 4 model with actuator (hold on its position by the clamp) and release spring.

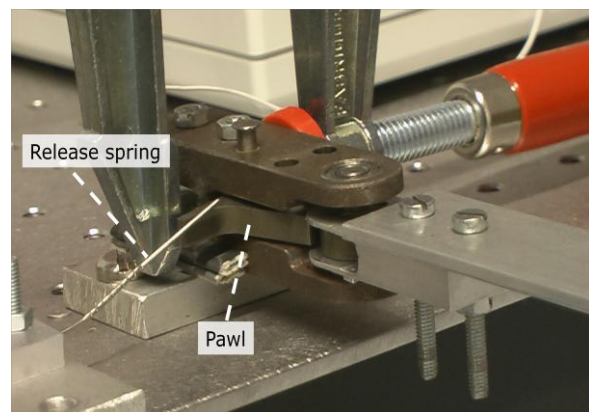


Figure 34: Detailed view where the pawl and release spring can be seen clearly.

5.6 Testing conclusions

5.6.1 Self-locking models

The only model that is consistently self-locking and reaches the locking torque of 2.0 Nm is the FA 4 model, with a contact angle of 7° and spiraled contact area.

The low contact angle of this final design was unexpected. This angle being 7° indicates that the friction coefficient is as low as:

$$a = \tan \alpha = \tan 7 = 0.12$$

With a the friction coefficient and α the contact angle.

5.6.2 Gear wheel mechanism

For the gear wheel models, it is clear to see that the second generation models perform better than the first generation models. The GW 3 model, which is an improvement on the GW 1 model, has slightly higher locking torque while requiring less actuation stroke. The GW 4 model, being a completely renewed design with lower contact angles but at the cost of a larger step size, has clearly the best performance of the gear wheel models. However, this performance is still not enough to achieve self-locking. However, a gear wheel with straight teeth and a contact angle of 7°, based on the result of the FA 4 model, might work.

The following conclusions can be made from the test results:

- Using only 2 teeth gives direction-independent locking torque. This can be seen because the GW 2 model has direction dependent locking behavior whereas the GW 3 and GW 4 models act direction independent.
- Using teeth with a lower contact angle helps to increase the locking torque. This is shown by the improvement of locking load for the GW 3 and, even more, the GW 4 models.
- The effect of the size of the teeth cannot be shown clearly.
- The effect of the shape of the teeth cannot be shown clearly. However, the sharp edges like in the GW 2 model do not give any advantage as they wear out easily.
- The locking torque of a non self-locking gear wheel mechanism is almost a linear function of the actuation force. This can be seen in the results for the GW 4 model with varying actuation force.

5.6.3 Friction amplifying mechanism

For the friction amplifying mechanism models, some results require some explanations. The FA 1 model was self-locking at its first tests, but very inconsistently and depending on the rotational orientation of the drum. A reason might be that the drum had a roundness outside its tolerances, leading to a locally lower contact angle with induced self-locking. Quick wear of the drum might have made the drum more concentric, leading to a more averaged contact angle being too high for self-locking.

The second generation FA 3 model, which is intended to be an improvement of the FA 1 model with the same parts, uses a drum with better concentric tolerances. However, the parts required such modifications, like shortening, that once the model reaches self-locking, it now is only capable of locking a torque up to 1.0 Nm. With higher torques, the lock will slam through with the friction pawl sliding past the drum.

The following conclusions can be made from the test results:

- The contact angle has to be below 10° to ensure self-locking.
- A contact angle of 10° and higher gives inconsistent self-locking capabilities, as can be seen from the results of the FA 5 model. However, a higher actuation force gives a higher chance of self-locking.
- In case of non self-locking models, the locking torque is not clearly dependent on the actuation force and can vary with the rotational orientation. This is shown by the results for the FA 5 model.
- A model with friction pawls with a spiraled contact area can handle play in the mechanism better than a model with friction pawls with a flat contact area.
- Play between the parts and deformations due to the high forces in the mechanism can give a significant locking compliance; e.g. that the joint rotates partly when locked and loaded.

6 Future design

6.1 Description of the joint design

Knowing now that the friction amplifying mechanism can give the best result, a renewed design is made for a future prototype, which is shown in figure 35. The design incorporates important aspects from the FA 4 functional model like the contact angle of 7° and a logarithmically spiraled contact area. A double friction pawl is included as well as a 110C 6V solenoid as linear actuator. Several changes compared to the functional models are explained as well as features that are added to get close to the actual design for the prosthetic fingers.

Also, a 2-fingered hand design has been made and is described in paragraph 6.4.

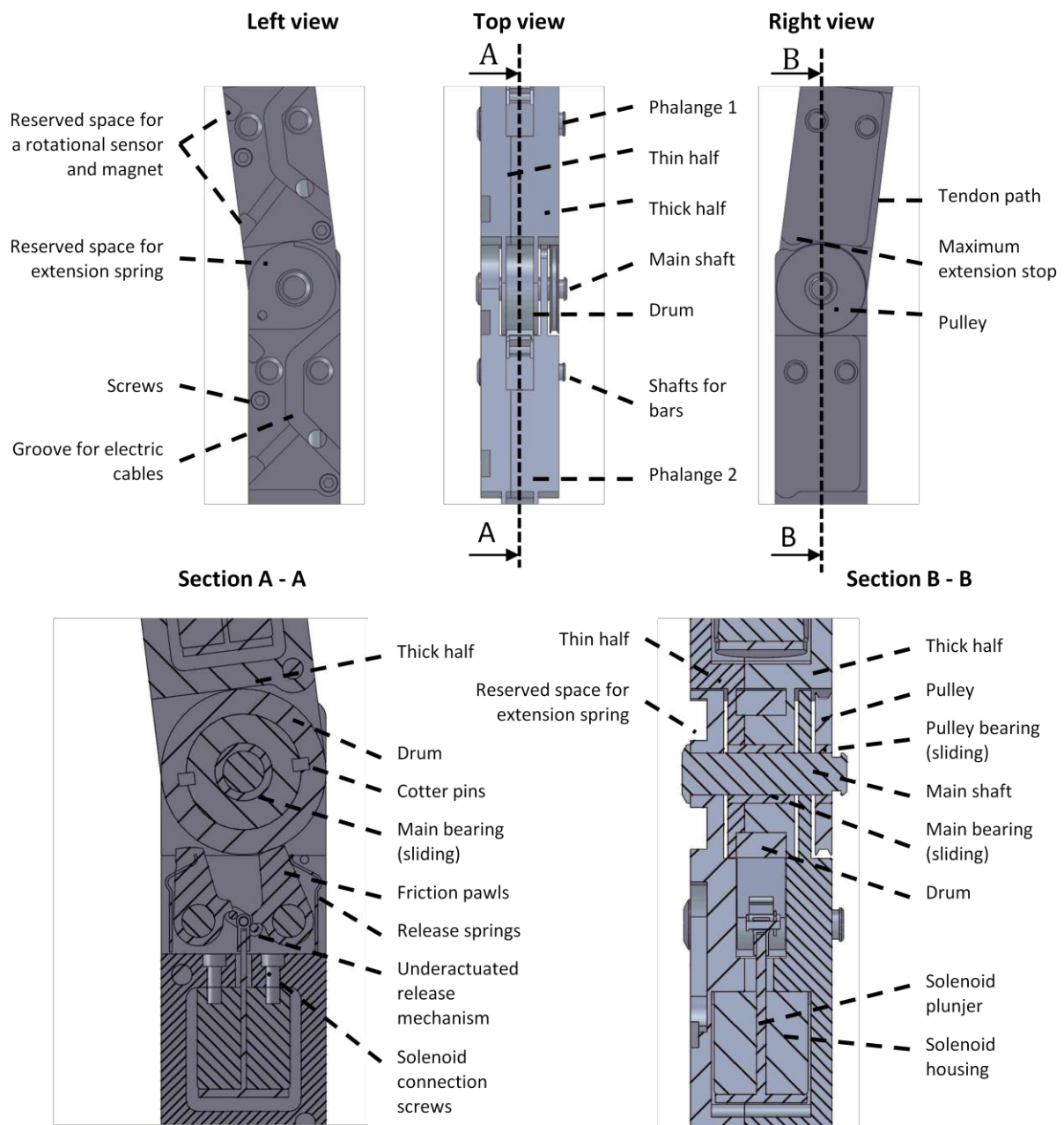


Figure 35: SolidWorks pictures and cross-sectional views of a single joint with 2 phalanges.

6.2 Extra features

For the future design, several features are included that were not required for the functional models. They are described below:

- A solenoid actuator is added in each finger to provide the control of the lock. Since the mechanism is normally closed, the actuator is only required to release the lock and allow for movement. The friction pawls are underactuated by a lever bar with 3 pins. The middle pin is pushed by the solenoid shaft, while the upper and lower pins will push the pawls. If one pawl is still locked due to an external load on the lock, at least the other pawl will be disengaged completely while keeping the release force on the first pawl. If then the external load is removed or changes direction, the first pawl will disengage and the lock will be released in both directions.
- Space is reserved for a rotational sensor which can be included later on. It is assumed that an electromagnetic sensor will be used, requiring a permanent magnet at the opposing phalange. Space is reserved for this magnet as well.
- A groove for electric cables is made at one side of the phalange, allowing the cables for the rotational sensor and the solenoid, as well as cables going to more distal phalanges. Crossing the joint, the cables will run at the dorsal side.
- The shafts for the friction pawls are designed as safety protection, meaning that if a higher external load is applied on the lock, they will break before any other part. According to the calculations in appendix G, the shafts will break with an external load of 6.4 Nm, so factor 3.2 higher than the required locking torque, when common structural steel is used. However, this situation is not desirable since the contact stresses on the pawl and the drum might be high enough to damage the contact areas of these parts.

6.3 Important design changes

The changes in the design compared to the functional models are described below.

- The contact angle is chosen as 7° and the contact area is designed as logarithmically spiraled, following from the FA 4 model. As a drawback, this contact angle gives high forces in the drum and the friction pawls.
- The diameter of the drum is increased to 20 mm. This reduces the required friction force of the friction pawls to the drum and therefore also the forces through the drum and pawls. Calculations for these forces are made in appendix G and give a friction force F_f of 200 N, a force through the drum of 2.2 kN and a force through the pawls of 2.2 kN.
- The bearings are replaced by a dry friction sliding bearing. Ball roller bearings would not be able to endure the high force through the drum to the main shaft but the sliding bearing used (the PCM 050708 E or B from SKF) in the design can handle static loads up to 10 kN. A dry friction sliding bearing is preferred over needle roller bearings since they do not require lubrication. Lubrication is unwanted anywhere in the finger since this can contaminate the drum or friction pawls and thus decrease the friction coefficient. Furthermore, the bearing is placed inside the drum to save space at the sides of the joint. The main shaft is thus

connected to phalange 2. The bearing is quite wide so it can handle finger sideway bending moments as well. Spacers between both phalanges will prevent axial movements.

- The drum is connected through cotter pins to phalange 1 instead of round pins to save radial space and make the connection stronger.
- The friction pawls are shorter, 8.9 mm, to reduce space and reduce flexibility due to compression of the pawls. Flexibility adds to the locking compliance and should therefore be kept low.
- The mechanism is normally closed, which means that the actuator is required to release the lock. The release springs are designed as small leaf springs located above and below the friction pawls. Each pawl has an independent release spring.
- The phalanges are split to fit the solenoid actuator inside. Screws and positioning edges are used to keep the 2 halves, a thick and a thin one, together.
- The pulley and extension spring are placed to the outside of the main shaft to allow a more rigid connection between the phalanges. Also, the tendon and spring can be accessed easier.
- The width of the phalanges is reduced by 4 mm to 19.8 mm. The height remains 20 mm.

For material choices, the drum and friction pawls should again be made from hardened steel. The main shaft can be from structural or high-strength steel, whereas the pawl shafts should be made from structural steel. The phalanges can be made from aluminum, although the strain due to the high forces might add to the locking compliance. In that case, steel phalange ends might work better due to the higher stiffness of the material.

6.4 Description of the 2-fingered hand design

The 2-fingered hand design with its actuation mechanism is shown in figure 36. The left finger has 3 active joints, which can be controlled by the solenoid actuators inside the phalanges. The right finger has 2 active joints, the MCP and PIP joints, and the DIP joint is coupled to the PIP joint. For this coupling, special pulleys are placed on the PIP and DIP joints, sticking out on the main shafts. This allows tendons to cross the middle phalange (MP). The tendons are connected to the proximal phalange (PP) at the bottom and the distal phalange (DP) at the top. With this configuration, the rotation of the DIP joint is directly coupled to the rotation of the PIP joint.

Furthermore, the tendon routing of the flexion tendon is shown where the tendon is connected to the DPs of both fingers. With using the DC motor and spindle drive as linear actuation mechanism, the configuration of the free moving pulley and the tendons on the pulleys act as underactuation for both the separate fingers as well as for the separate phalanges in a single finger.

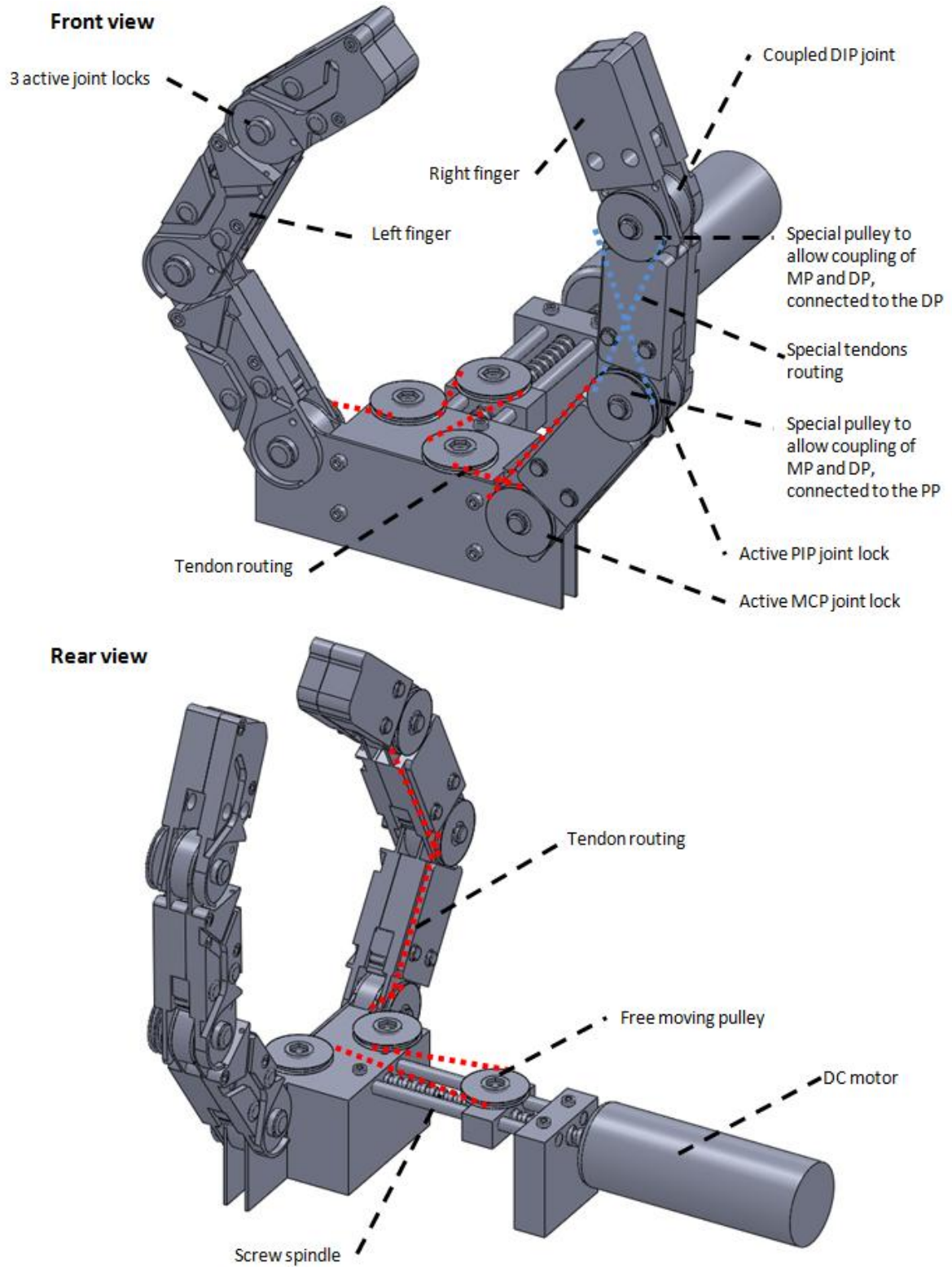


Figure 36: SolidWorks pictures of the 2-fingered hand with actuation mechanism.

Figure 37 shows 3 different gestures from the 2-fingered hand as examples. The only limitations for different gestures for this future design hand are the coupling of the PIP and DIP joints in the right finger and the 90° flexion limitation for each joint.



Figure 37: 3 different gestures that are possible with the 2-fingered hand design.

7 Conclusion and recommendations

7.1 Conclusion

In this assignment the potentials for joint locks in an underactuated prosthetic hand are reviewed. Functions and requirements for such a lock are set and several locks are investigated. Two concepts are developed further and tested with functional models. The friction amplifying mechanism gives the best locking performance with self-locking behavior, requiring only a small actuation force. A future design of this lock including a 2-fingered hand is designed and can be used for future work. However, the manufacturing and testing of this hand was not possible within the time for this assignment.

From comparing the developed lock to the functions set in chapter 2, being preventing motion between 2 phalanges, releasing the lock and measuring the rotational position, it follows that the first and second are met with the functional model. The third function can easily be included in the future design.

The requirements from chapter 2 are the following:

- 1) Withstand 2.0 Newton meter of torque, 200 Newton of axial force and 20 Newton of radial force.

This requirement is met in the functional model and future design. The locking torque has been proved with testing.

- 2) A torque overload protection mechanism is included, which protects the important parts for torques above 6.0 Newton meter.

There is no non-destructive overload protection mechanism developed for the joint lock. However, some parts that can be replaced easily are designed as safety protection, with a calculated maximum torque of 6.4 Nm.

- 3) Locking is possible in both directions.

This requirement is met in the future design.

- 4) Locking and releasing can be done with a single actuator.

This requirement is met in the future design.

- 5) The lock should have an angular tolerance under 3°.

This requirement is not met in the functional model, as been proved by testing that the angular tolerance reaches 14°. Improvements are made in the future design but the effect has to be investigated.

- 6) Maximum dimensions are comparable with MCP joint dimensions: breadth (medial – lateral direction) 25 mm and depth (palmar – dorsal direction) 30 mm.

The dimensions in the functional model and the future design are well below the maximum dimensions stated in this requirement.

- 7) Favorable dimensions are comparable with PIP joint dimensions: breadth (medial – lateral direction) 18 mm and depth (palmar – dorsal direction) 17 mm.

The dimensions in the future design are slightly above the dimensions stated in this requirement. However, for the PIP and DIP joints, the locks can expect lower locking torques. Redesign of these specific locks can result in lower dimensions.

- 8) The lock can be operated from -10°C to $+40^{\circ}\text{C}$.

This requirement is not investigated or tested.

At the end of the line, most functions and requirements are either met in the functional model or included in the future design. The missing requirements are therefore included in the recommendations, along with possible improvements of the lock.

7.2 Further recommendations

From all the experiences throughout the process and plans for the design that were beyond the time of this assignment, several recommendations are made. They include advice on the using the current future design model but also steps to take for implementation in the complete hand prosthesis.

- Find a material combination or coatings for the drum and friction pawls that provides a higher and consistent friction coefficient. These materials or coatings should be at least as stiff and resistant against wear as the current hardened steel. Then, redesign the diameter of the drum and / or the contact area of the pawls with a contact angle that suits the new friction coefficient. With this redesign, smaller forces inside the finger will be required and the height restriction that comes from the current drum diameter can be reduced.
- Protect the locking mechanism against contamination from outside since this might reduce the friction coefficient or increase the wear of the drum and friction pawls.
- Do extensive tests with a lock to find the rate of wear and decide whether this is acceptable or not.
- Redesign the DIP and PIP locks for lower locking torque and smaller dimensions.
- Redesign the phalanges as lightweight and test whether they remain strong enough for the high loads in the mechanism.

- The dimensions of the phalanges are now limited by the size of the actuator. To be able to build the phalanges smaller, search for and test possible other actuators that are smaller than the solenoid, but still as reliable.
- When redesign of the joint lock is finished and specifications, like the required dimensions, weight, performance, energy consumption and more, are known, decide which joints should include a lock and which joints should be passively coupled to other joints.

Appendix A: Analysis of phases during forming of grasp types

When the fingers of the hand obtain the different grasps, several phases are needed where the different fingers either move or their hold positions. Analyzing the grasps gives insight on the specific phases that are found in the different grasp types which gives information about the need of independent actuation and locking. From these phases, basically only during the holding phases the locks will be active.

A. Key grasp

Movement

1. Opposition thumb (if needed; to dorsal side).
2. Holding thumb.
3. Flexion index, middle, ring and little finger.

Active loading

4. Flexion thumb.

B. Tripod grasp

Movement, no loading

1. Opposition thumb (to palmar side).
2. Holding thumb, middle and index finger.
3. Flexion little and ring finger.
4. Flexion index and middle finger.

Reactive loading

5. Holding index and middle finger; loaded on fingertip.

Active loading

6. Flexion thumb; loaded on fingertip.

C. Cylindrical grasp

Movement, no loading

1. Opposition thumb (to palmar side).
2. Holding thumb.

Active loading

3. Flexion index, middle, ring and little finger.

4. Flexion thumb.

D. Finger point

Movement, no loading

1. Holding index finger, thumb.
2. Flexion middle, ring and little finger.
3. Flexion thumb.

Loading

None...

Appendix B: Free body analysis of the finger

A free body analysis will show the static torques and forces on the joints with joint angles and tendon forces as variables. In this analysis, a constant fingertip force of 20 Newton is applied perpendicular on the tip of the distal phalange, analyzing the most extreme situation of the tripod grasp. The tendon force is varied from 0 to 200 Newton, as explained below, and the joint angles vary from 0° to 90° each. The results are calculated with a Matlab script. Free body diagrams are shown in figure 38 to 43 that are the basis for the equilibrium equations.

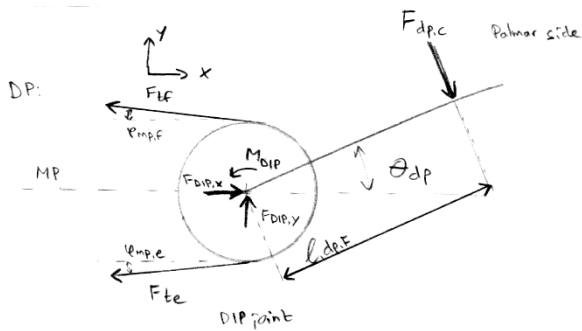


Figure 38: Free body diagram for the distal phalange.

Unknown: M_{dip} ; $F_{dip,x}$; $F_{dip,y}$

$$\sum M = 0 = F_{dp,c} \cdot l_{dp,f} + F_{te} \cdot r_{dip,e} - F_{tf} \cdot r_{dip,f} - M_{dip}$$

$$\sum F_x = 0 = F_{dip,x} + F_{dp,c} \cdot \sin \theta_{dp} - F_{tf} \cdot \cos \varphi_{mp,f} - F_{te} \cdot \cos \varphi_{mp,e}$$

$$\sum F_y = 0 = F_{dip,y} - F_{dp,c} \cdot \cos \theta_{dp} + F_{tf} \cdot \sin \varphi_{mp,f} - F_{te} \cdot \sin \varphi_{mp,e}$$

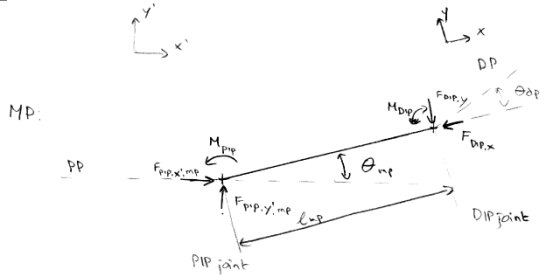


Figure 39: Free body diagram for the middle phalange.

Unknown: M_{pip} ; $F_{pip,x',mp}$; $F_{pip,y',mp}$

$$\sum M = 0 = F_{dip,y} \cdot l_{mp} - M_{pip} + M_{dip}$$

$$\sum F_{x'} = 0 = F_{pip,x',mp} - F_{dip,x} \cdot \cos \theta_{mp} + F_{dip,y} \cdot \sin \theta_{mp}$$

$$\sum F_{y'} = 0 = F_{pip,y',mp} - F_{dip,y} \cdot \cos \theta_{mp} - F_{dip,x} \cdot \sin \theta_{mp}$$

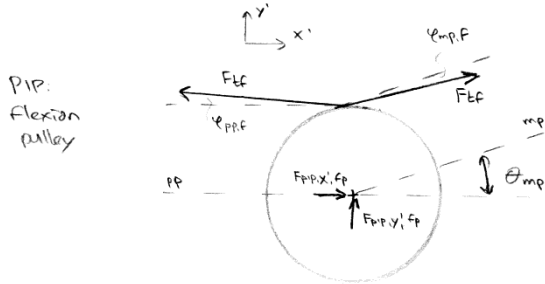


Figure 40: Free body diagram for the idle flexion pulley on the PIP joint.

Unknown: $F_{pip,x',fp}$; $F_{pip,y',fp}$

$$\sum F_{x'} = 0 = F_{pip,x',fp} + F_{tf} \cdot \cos(\theta_{mp} - \varphi_{mp,f}) - F_{tf} \cdot \cos \varphi_{pp,f}$$

$$\sum F_{y'} = 0 = F_{pip,y',fp} + F_{tf} \cdot \sin(\theta_{mp} - \varphi_{mp,f}) - F_{tf} \cdot \sin \varphi_{pp,f}$$

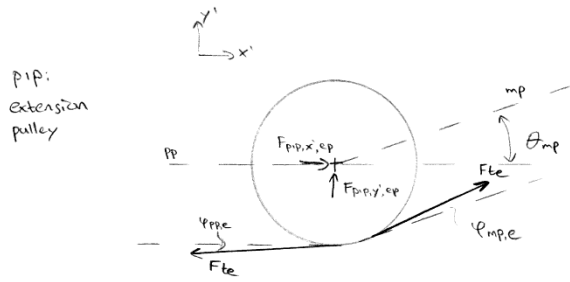


Figure 41: Free body diagram for the idle extension pulley on the PIP joint.

Unknown: $F_{pip,x',ep}$; $F_{pip,y',ep}$

$$\sum F_{x'} = 0 = F_{pip,x',ep} + F_{te} \cdot \cos(\theta_{mp} - \varphi_{mp,e}) - F_{te} \cdot \cos \varphi_{pp,e}$$

$$\sum F_{y'} = 0 = F_{pip,y',ep} + F_{te} \cdot \sin(\theta_{mp} - \varphi_{mp,e}) - F_{te} \cdot \sin \varphi_{pp,e}$$

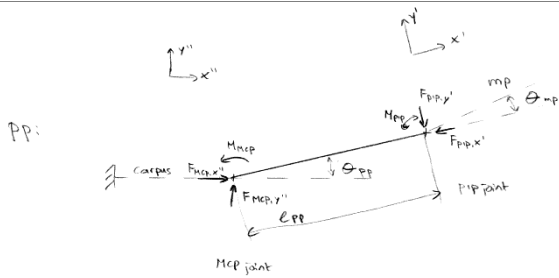


Figure 42: Free body diagram for the proximal phalanx.

Unknown: M_{cp} ; $F_{mcp,x''}$; $F_{mcp,y''}$

$$\sum M = 0 = F_{dip,y'} \cdot l_{pp} - M_{mcp} + M_{pip}$$

$$\sum F_{x''} = 0 = F_{mcp,x''} - F_{pip,x'} \cdot \cos \theta_{pp} + F_{pip,y'} \cdot \sin \theta_{pp}$$

$$\sum F_{y''} = 0 = F_{mcp,y''} - F_{pip,y'} \cdot \cos \theta_{pp} - F_{pip,x'} \cdot \sin \theta_{pp}$$

With:

$$F_{pip,x'} = F_{pip,x',mp} + F_{pip,x',fp} + F_{pip,x',ep}$$

$$F_{pip,y'} = F_{pip,y',mp} + F_{pip,y',fp} + F_{pip,y',ep}$$

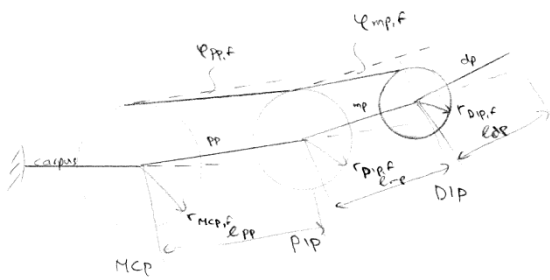


Figure 43: Schematic view of the finger to show ϕ angles.

$$\varphi_{mp,f} \approx \tan^{-1} \frac{r_{pip,f} - r_{dip,f}}{l_{mp}}$$

$$\varphi_{pp,f} \approx \tan^{-1} \frac{r_{mcp,f} - r_{pip,f}}{l_{pp}}$$

Similar:

$$\varphi_{mp,e} \approx \tan^{-1} \frac{r_{pip,e} - r_{dip,e}}{l_{mp}}$$

$$\varphi_{pp,e} \approx \tan^{-1} \frac{r_{mcp,e} - r_{pip,e}}{l_{pp}}$$

The joint torques for the different joints are shown in figures 44 to 46 with using a tendon force of 100 Newton. The main influence of varying the tendon force is shifting the graphs up and down. The MCP joint angle had no influence on the joint torques as expected, so for clarification this variable is not shown. It is clear that full extension of the DIP and PIP joint give maximum values while full

flexion give minimum values. It is therefore convenient to plot the joint torques at full extension and full flexion as functions of the tendon force, as shown in figures 47 - 49.

The maximum tendon force can be found when assuming a maximum tripod grasp of 20 N, where the index and middle finger are locked and the thumb has locked PIP and DIP joints, so only rotating around its MCP joint. In this case only 1 joint can rotate freely and the torque put on this joint is caused by the flexion tendon in this finger. The torque required on this joint equals the tip force multiplied by the finger length: $20 \text{ N} * 100 \text{ mm} = 2.0 \text{ Nm}$. The torque caused by the tendon force on the flexion tendon pulley must be the same. When assuming a pulley radius of 10 mm, this requires a tendon force of $2.0 \text{ Nm} / 10 \text{ mm} = 200 \text{ N}$.

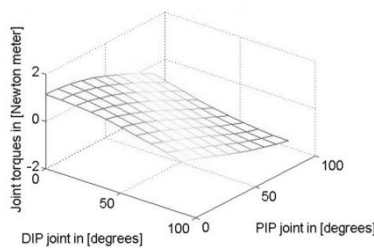


Figure 44: Joint torques in MCP joint with a tendon force of 100 N.

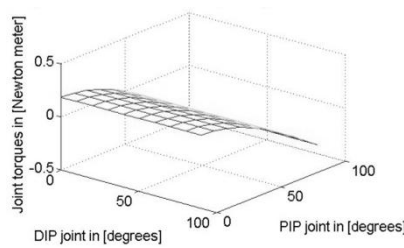


Figure 45: Joint torques in PIP joint with a tendon force of 100 N.

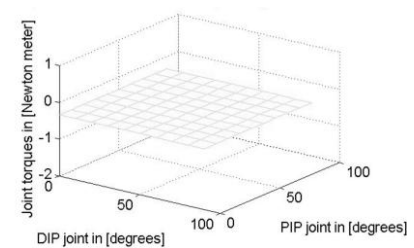


Figure 46: Joint torques in DIP joint with a tendon force of 100 N.

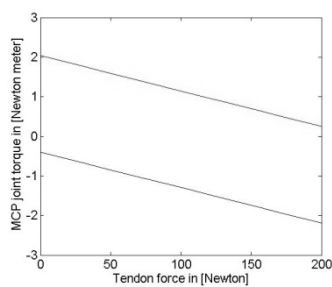


Figure 47: Joint torques in MCP joint as function of the tendon force. Blue: maximum value; black: minimum value.

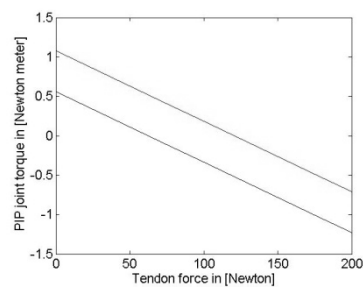


Figure 48: Joint torques in PIP joint as function of the tendon force. Blue: maximum value; black: minimum value.

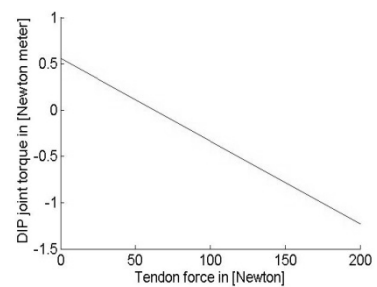


Figure 49: Joint torques in DIP joint as function of the tendon force. The torque is independent on joint angles.

It can be concluded that the MCP joint lock has to withstand a joint torque of ± 2.0 Newton meter, the PIP joint lock a torque of ± 1.2 Newton meter and the DIP joint lock a torque of maximal 0.6 and minimal -1.2 Newton meter. Even though fine-tuning the tendon force can reduce the average joint locking torque, still the influence of the varying joint angles is too large to take the risk of lowering the specifications of the locking torque below the maximum achievable joint torques.

In a similar way results can be obtained for the joint forces in radial and axial directions. Figure 50 shows the joint forces in axial direction for the MCP joint with a tendon force of 100 Newton and varying DIP and PIP joint angles. Figure 51 shows the maximum and minimum joint forces for varying tendon forces.

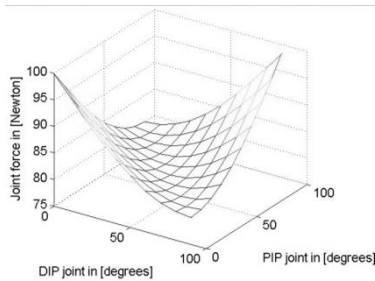


Figure 50: Joint forces in axial direction in MCP joint with a tendon force of 100 N.

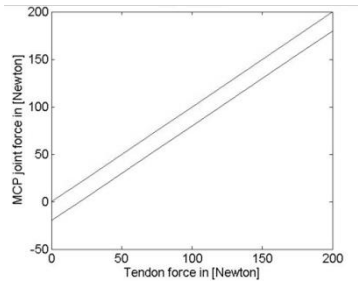


Figure 51: Joint forces in axial direction in MCP joint as function of the tendon force. Blue: maximum value; black: minimum value.

Joint forces in the DIP and PIP joints appear to be the same as in the MCP joint. Furthermore, the joint forces in radial direction are between ± 20 Newton for all joints. Thus, for a tripod grasp of 20 Newton a maximum joint force of 200 Newton can be expected. Running the calculations with a grasping force of 100 Newton, the maximum force does not exceed 200 Newton although the minimum force is -100 Newton. This indicates that for other grasp types with loads up to 100 Newton combined on all phalanges the joint forces will not grow excessively.

Appendix C: Calculations for the concepts

Concept A: Gear wheel

Module: relating diameter to module to indexing resolution

The module of a gear wheel is defined by

$$mod = \frac{D_{eff}}{N}$$

with D_{eff} the effective diameter and with N the number of teeth. The lower limit of modules to be manufactured is around 0.2. With this module a gear wheel of 20 mm diameter will have 100 teeth. The indexing resolution is thus

$$resolution = \frac{360^\circ}{N}$$

in this case the resolution will be 3.6° .

Calculating a as function of alpha, showing the concept should be self-locking

In figure 52, a simplified free body diagram of the gear wheel with contact to the gear pawl is shown.

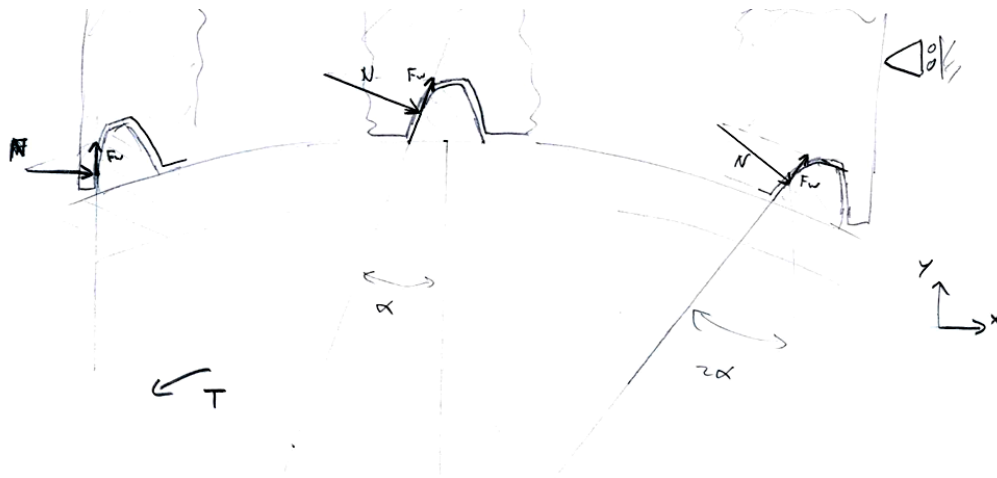


Figure 52: Simplified free body diagram of the gear wheel teeth

$$\sum F_y = 0 = -F_f + N \cdot \sin \alpha - F_f \cdot \cos \alpha + N \cdot \sin 2\alpha - F_f \cdot \cos 2\alpha$$

with F_f is the friction force along the teeth, N the normal force on the teeth and α the angle of contact of the teeth.

When rewriting F_f as

$$F_f = a \cdot N$$

then the ratio between the normal force and the friction force can be calculated as:

$$a = \frac{\sin \alpha + \sin 2\alpha}{1 + \cos \alpha + \cos 2\alpha}$$

With using an angle of $\alpha = 20^\circ$, it follows that $a = 0.36$. This is below the usual friction coefficient of steel to steel, implying that the concept will be self-locking.

Calculating shear stress in teeth

The average force on a single tooth can be calculated with

$$F_{st} = \frac{T}{N \cdot r}$$

With T the locking torque, N the number of teeth in contact and r the radius of the gear wheel. Assuming a locking torque of 2.0 Nm, 20 teeth in contact and a radius of 10 mm, the average contact force on a single tooth is 10 N.

The average shear stress in a tooth can be calculated with

$$\sigma_{average} = \frac{F_{st}}{w \cdot t}$$

where w is the width of a tooth and t is the thickness of the gear wheel. With a width of 0.6 mm and thickness of 3 mm, the average shear stress is 5.3 MPa. Assuming the maximal shear stress to be 5 times the average shear stress, the maximum shear stress will be 26.5 MPa.

Concept B: Friction amplifying mechanism

Calculating a as function of α

Figure 53 shows a free body diagram of a linear friction amplifying mechanism. The principle is similar to the rotational mechanism and can be used as a simplification to calculate the influence of the angle α on the friction coefficient.

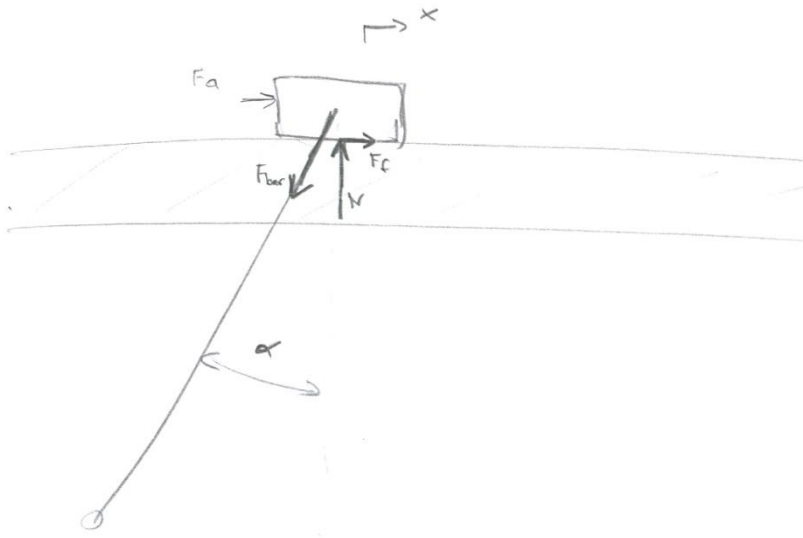


Figure 53: Free body diagram of a linear friction amplifying mechanism

The actuation force is required to push the friction pad to the sliding disc. Assuming the mechanism to be self-locking, the actuation force can then be disregarded. Then, the amplitude of the friction force F_f can be formulated as

$$F_f = F_{bar} \cdot \sin \alpha$$

and the amplitude of the normal force N as

$$N = F_{bar} \cdot \cos \alpha$$

with F_{bar} is the tension force in the bar in the direction of the joint of the bar. Therefore, the following relation between F_f and N exists:

$$F_f = N \cdot \tan \alpha$$

When again rewriting F_f as

$$F_f = a \cdot N$$

it follows that

$$a = \tan \alpha$$

In case of an angle α of 15° , this results in an α of 0.27. This is below the static friction coefficient for clean steel on steel, concluding that the mechanism will be self-locking.

For the concept, the friction force has to be:

$$F_f = \frac{T}{r}$$

with T is the locking torque and r the radius of the wheel. Assuming a locking torque of 2.0 Nm and a radius of 7.5 mm, the friction force has to be 267 N. Using an angle α of 15° , according to the above equations the force in the bar will become 1.03 kN.

Concept C: Band brake

Simplified capstan equation

The ratio of tension forces at both sides of the band can be calculated with: <reference>

$$F_1 = F_2 \cdot e^{\mu \cdot \vartheta}$$

where F_1 and F_2 the forces at both ends, μ the friction coefficient between the band and the drum and ϑ the angle of contact in radians. If $F_1 \gg F_2$, the locking torque will be:

$$T = F_1 \cdot r$$

with r the radius of the drum. With assuming a radius of 7.5 mm and μ between 0.4 and 0.7 and taking different angles θ , the following actuation forces would be required:

μ	ϑ	F_2
0.4	2π	22 N
0.4	6π	0.14 N
0.4	10π	$0.9 \cdot 10^{-3}$ N
0.7	2π	3.3 N
0.7	6π	$0.5 \cdot 10^{-3}$ N
0.7	10π	$81 \cdot 10^{-9}$ N

Concept D: Axial wedge

Relation μ_{low} , μ_{high} and friction force

Figure 54 shows a free body diagram of a linear wedge, with at the top a sloped plate, representing the curved disc, and at the bottom a flat plate, representing the flat disc. Here is α the angle of the wedge, N_1 the normal force on the curved side of the wedge, F_{w1} the friction force on the curved side, N_2 the normal force on the flat side and F_{w2} the friction force on the flat side.

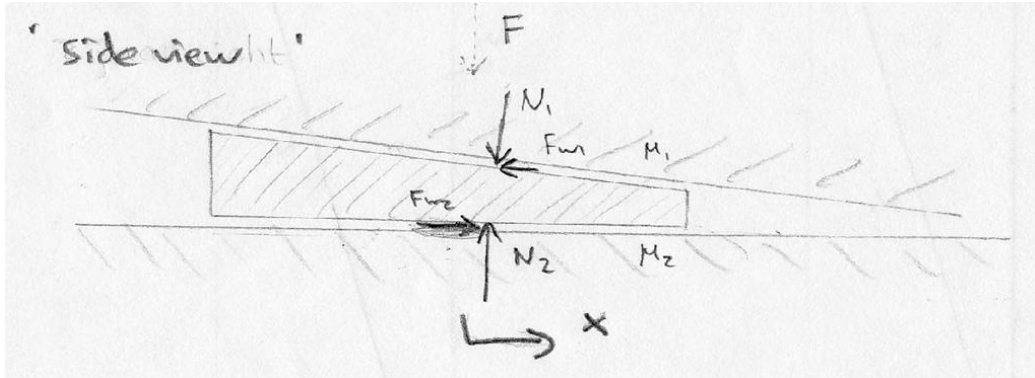


Figure 54: Free body diagram of a linear wedge.

The mechanism works with slipping at the curved side, so:

$$F_{w1} = \mu_{1,d} \cdot N_1$$

Further, F_{w2} transmits the locking torque, so

$$F_{w2} = \frac{T}{r}$$

with T the locking torque and r the radius of the discs. Also, there are the geometric equations:

$$F_{w2} = F_{w1} \cdot \cos \alpha + N_1 \cdot \sin \alpha$$

and

$$N_2 = N_1 \cdot \cos \alpha - F_{w1} \cdot \sin \alpha$$

The mechanism requires static friction on the flat disc, so

$$F_{w2} = a \cdot N_2$$

with $a < \mu_{2,s}$.

This a can thus be found with

$$a = \frac{F_{w2}}{N_2} = \frac{F_{w1} \cdot \cos \alpha + N_1 \cdot \sin \alpha}{N_1 \cdot \cos \alpha - F_{w1} \cdot \sin \alpha} = \frac{\mu_{1,d} \cdot \cos \alpha + \sin \alpha}{\cos \alpha - \mu_{1,d} \cdot \sin \alpha}$$

For different values of $\mu_{1,d}$ and α , a and N_2 are:

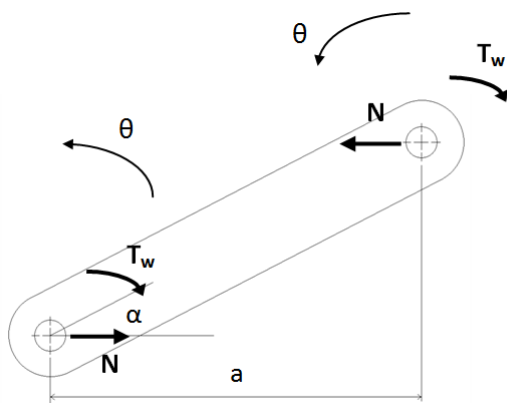
$\mu_{1,d}$	α	a	N_2
0.2	5°	0.29	911 N
0.2	10°	0.39	683 N
0.2	15°	0.49	539 N
0.4	5°	0.51	528 N
0.4	10°	0.62	430 N
0.4	15°	0.75	356 N

This table shows that a friction coefficient $\mu_{1,d}$ of 0.4 and up and an angle α of 10° and up will require a $\mu_{2,s}$ of well above 0.5. This might be impossible to guaranty so it would be recommended to stay below these values for $\mu_{1,d}$ and α .

Forces in knee-lever

The figures and equations below show the static friction coefficients of the pins to the levers and actuation and release forces in equilibrium situations. Therefore the actual actuation and release forces should be larger to ensure movement of the actuation mechanism.

Holding phase



Calculating critical c'

$$\sum M = 0 = N \cdot a \cdot \sin \alpha - 2T_w$$

$$N \cdot a \cdot \sin \alpha = 2 \cdot c' \cdot N \cdot r$$

$$c' = \frac{a \cdot \sin \alpha}{2r} = 3 \sin \alpha$$

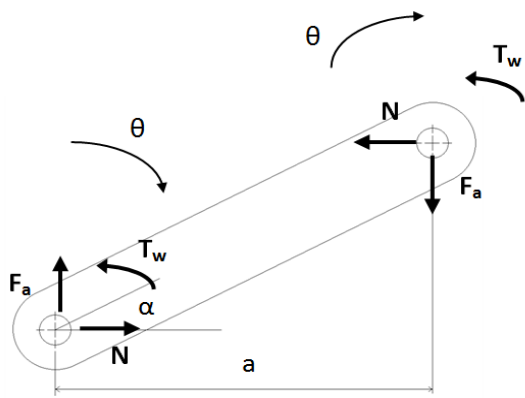
With: r the radius of the pin: $r = \frac{a}{6}$

Actuation phase

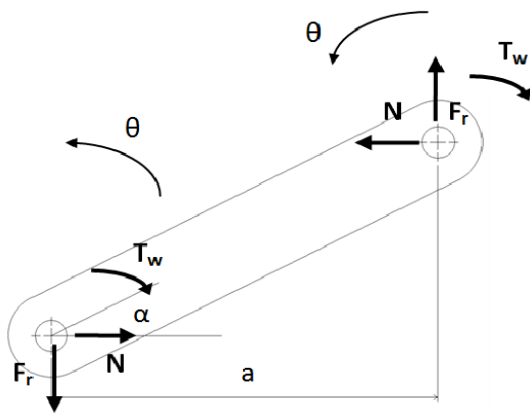
$$T_w = c \cdot N \cdot r$$

$$\sum M = 0 = N \cdot a \cdot \sin \alpha + 2T_w - F_a \cdot a \cdot \cos \alpha$$

$$F_a = \frac{N \cdot a \cdot \sin \alpha + 2c \cdot N \cdot r}{a \cdot \cos \alpha} = N \frac{\sin \alpha + \frac{1}{3}c}{\cos \alpha}$$



Releasing phase



$$\sum M = 0 = N \cdot a \cdot \sin \alpha + F_r \cdot a \cdot \cos \alpha - 2T_w$$

$$F_r = \frac{-N \cdot a \cdot \sin \alpha + 2c \cdot N \cdot r}{a \cdot \cos \alpha}$$

$$= N \frac{-\sin \alpha + \frac{1}{3}c}{\cos \alpha}$$

The following table shows the critical values for c' for different angles α .

α	c'
2.5°	0.13
5°	0.26
7.5°	0.39
10°	0.52

With using $\alpha = 5^\circ$ and $c = 0.4$, the actuation and release forces are linear functions of the actuated normal force respectively the remaining normal force:

$$F_a = 0.31N$$

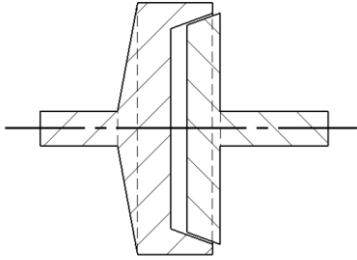
$$F_r = 0.046N$$

With a high remaining normal force, for example 600 N, the release force will need to be 28 N.

Appendix D: Other concepts

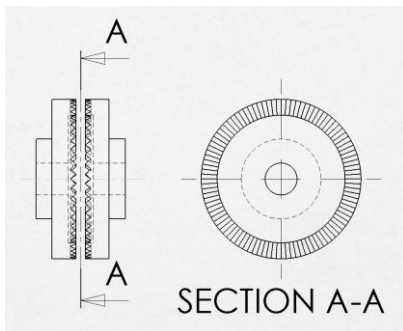
The concepts that were considered but rejected in an early stage of the concept selection process are listed below. For each concept, a short description and reason for rejection are given.

Cone clutch



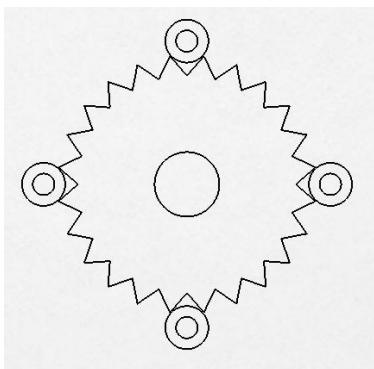
The cone clutch consists of an inner and outer cone, where the inner cone is pushed in axial direction to the outer cone. Decreasing the angle α of the slope of the cone increases the locking torque. However, a lock with optimal geometry and maximal dimensions cannot provide the required locking torque.

Axially toothed double plate with force closure



This concept has axially 2 toothed plates that are pushed together. The angle of the teeth is such flat that it has no self-locking but relies on the actuation force. Therefore the mechanism has an internal torque overload protection but the required actuation force is very high.

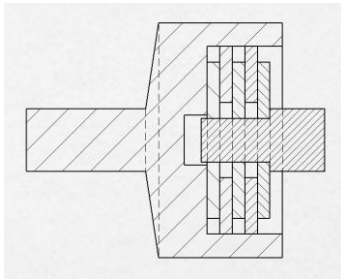
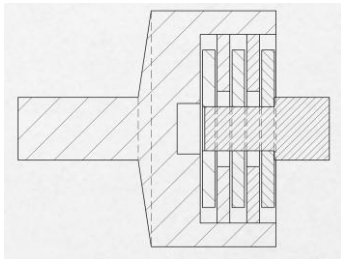
Arrêteringen



The arrêteringen concept consists of a gear wheel with small wheels pushed in the teeth. This concept cannot provide the required locking torque with allowable dimensions, is quite complex and has a rough indexing resolution.

The multiple disc clutch consists of disc that are

Multiple disc clutch

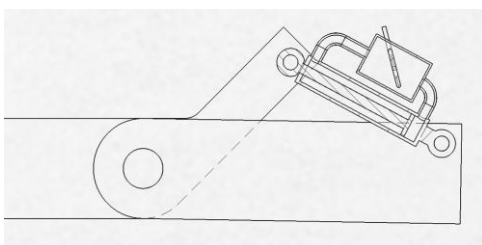


connected to the outer bus or the inner axis but remain free in axial direction. When locked, the discs are pushed together and transmit torque on each contact area. The more discs are included the higher the locking torque will be. However, with the allowable dimensions the required locking torque cannot be met.

Magnetorheological clutch

The Magnetorheological clutch is similar to the multiple disc clutch as it has discs connected to the outer bus and inner axis but a magnetorheological fluid is included in the mechanism. This fluid changes visco-elastic properties when put in a magnetic field. Changing the magnetic field can thus change the stiffness of the lock. But again, within the allowable dimensions the required locking torque cannot be met. <reference; <reference: paper about MR fluid joint lock>

Hydraulic or pneumatic clutch



The hydraulic or pneumatic clutch consists of a cylinder and piston connected to both phalanges. A connection between both ends of the cylinder with a valve controls the locking. When the valve is open, fluid or air can move between both ends of the cylinder, allowing the piston to move. When the valve is closed, the fluid or air cannot move and movement of the piston will be resisted. The main problem with this concept is the very high pressure in the cylinder, causing problems for the seals.

Appendix E: 3D printed plastic models

Explain a little about the 3D printed models; why we made them, how they were tested, etc.

Gear wheel mechanism

Before the functional models were built, a larger scale 3D printed plastic model was made, as can be seen in figure 55. Even though the main purpose was demonstration of the principle, this model was tested on its self-locking ability and this proved to work well. When the gear pawls were actuated and a locking torque was applied on the mechanism, the actuation force could be removed while the mechanism would remain locked. When increasing the locking torque the mechanism would still hold. Removing the locking torque caused the gear pawls to flip back to their original positions and thus release the mechanism.

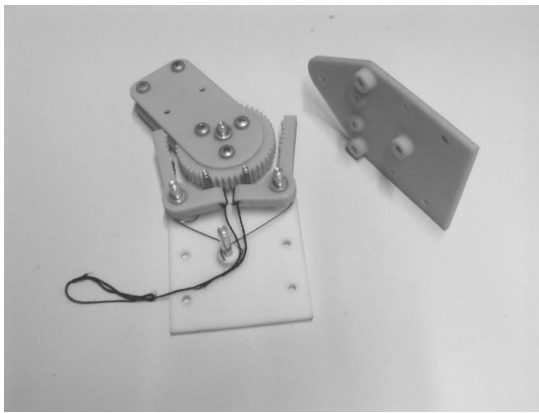


Figure 55: Picture of the gear wheel 3D printed model.

Friction amplifying mechanism

Just as for the gear wheel concept, a larger scale 3D printed plastic model was made as can be seen in figure 56. Unfortunately, the model did not self-lock since the friction coefficient was apparently too low. The locking torque was thus dependent on the actuation force but was very limited.

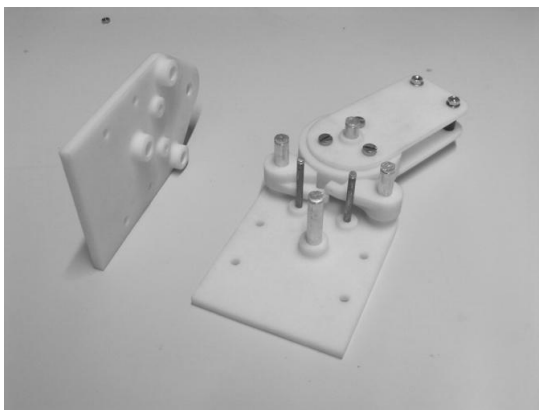


Figure 56: Picture of the friction amplifying mechanism 3D printed model.

Appendix F: Calculations for the functional models

FEM analysis for the gear wheel model

A quick FEM analysis has been done to find the maximum von Mises stresses in the gear pawl. The analysis has been carried out twice with a coarse and a fine mesh. The coarse mesh is shown in figure 57 and seems to cover the part well. At the small teeth, where lots of edges are present, the elements are much smaller. The hole for the shaft is regarded fixed, and forces are applied on the tooth sides in counter clock-wise rotation direction.

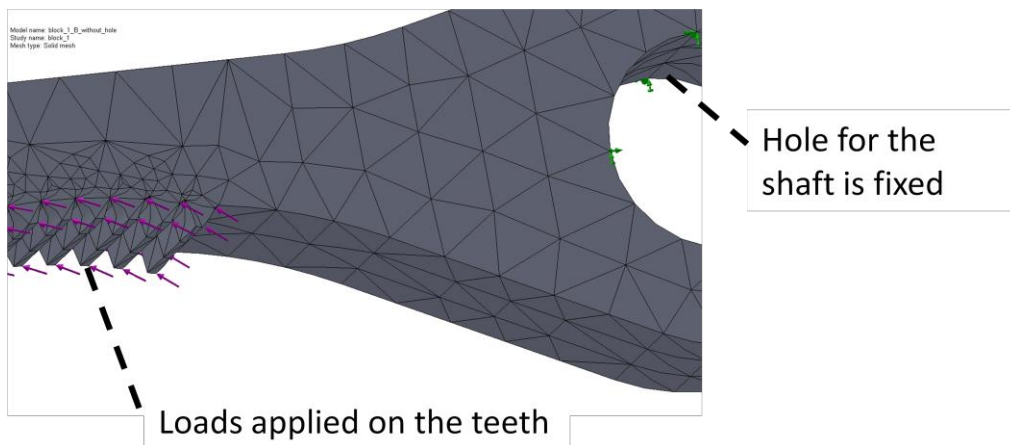


Figure 57: Coarse mesh of the gear pawl from the GW 1 model.

The results are shown in figure 58. It shows that the stresses might reach 290 MPa locally, just below the yield stress of machine steel, but only at very small concentrations on edges which is due to the way that a FEM handles small edges. However, the maximum stresses in the part are not expected to exceed 160 MPa.

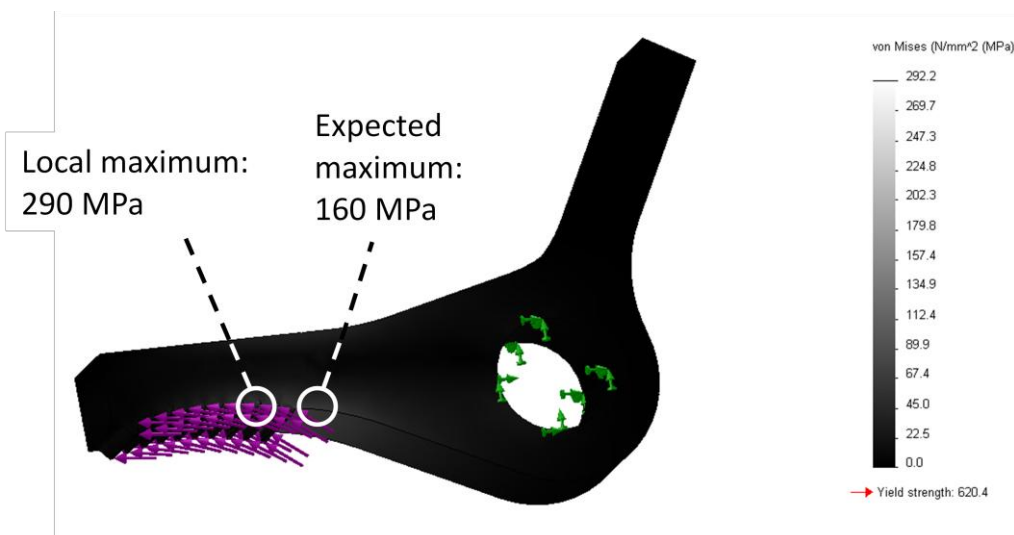


Figure 58: Von Mises stresses in the gear pawl at maximum load on the teeth. A FEM analysis using the SolidWorks Simulation tool.

The coarse mesh, used for this analysis, has 3503 elements and 6094 nodes. The fine mesh used for verification, has 32549 elements and 49579 nodes. The results from this verification are very similar to the first results, indicating that the coarse mesh was chosen well.

FEM analysis for the friction amplifying mechanism

For the friction amplifying mechanism is also a FEM analysis done, to find the maximum von Mises stresses in the friction pawls. The coarse mesh is shown in figure 59 and seems to cover the part well. The hole for the rotation shaft is regarded as fixed, while the normal force is applied on the contact surface.

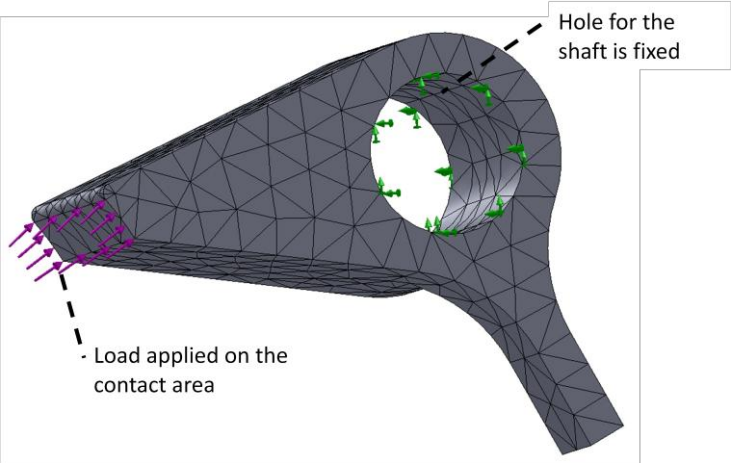


Figure 59: Coarse mesh of the friction pawl from the FA 1 model.

Figure 60 shows the result of such an analysis with a pawl with a contact angle of 18°, resulting in the high normal force of 820 N. The maximum stress in the design will become 180 MPa, well below the allowable maximum stresses of a common steel alloy.

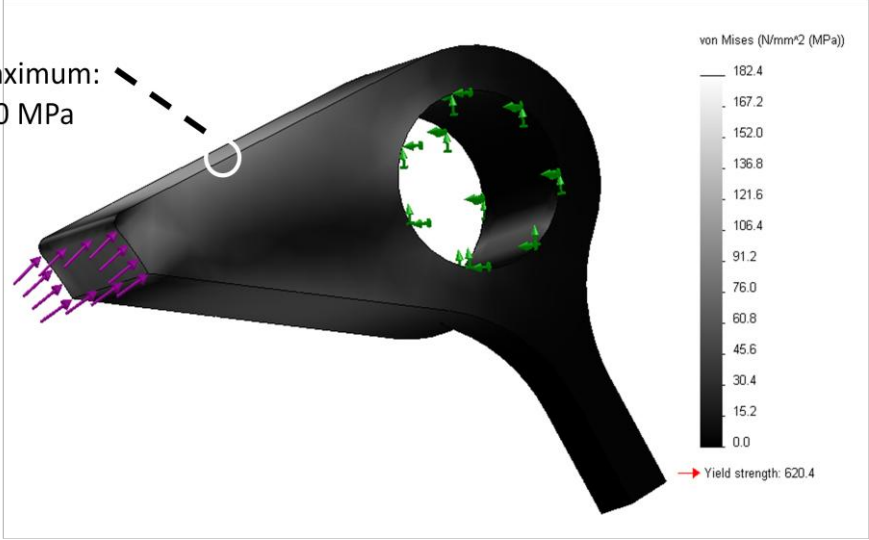


Figure 60: Von Mises stresses in the push pawl with a contact angle of 18° and at maximum load of 820 N. A FEM analysis using the SolidWorks Simulation tool.

The coarse mesh, used for this analysis, has 1546 elements and 2796 nodes. The fine mesh used for verification, has 27064 elements and 41155 nodes. The results from this verification are very similar to the first results, indicating that the coarse mesh was chosen well.

Hertzian contact stresses between the drum and the push pawls of the friction amplifying mechanism

The Hertzian contact stress for 2 parallel cylinders can be calculated with ^[17]:

$$p_0 = \sqrt{\frac{E^* \cdot F}{\pi \cdot L \cdot R}}$$

$$\frac{1}{R} = \frac{1}{R_1} + \frac{1}{R_2}$$

$$\frac{1}{E^*} = \frac{1 - \nu_1^2}{E_1} + \frac{1 - \nu_2^2}{E_2}$$

where p_0 is the maximum contact stress, F is the contact force, L is the length of the contact area, R_i are the radii of the contact bodies, E_i are the elastic moduli of the materials and ν_i are the poisson's ratio's of the materials.

The contact stress is calculated with material properties of steel for both parts, where $E = 210 \text{ GPa}$ and $\nu = 0.3$. The radius is 7.5 mm for the drum and 10^9 mm for the push pawl, approaching a flat surface. The contact force is 820 N , being the highest contact force in case of an 18° contact angle. With these variables, the maximum contact stress reaches 900 MPa which is quite high but probably below the allowable contact stress for machine steel.

Furthermore, the indentation depth might have an influence on the change of geometry of the mechanism and can be calculated with:

$$F = \frac{\pi}{4} E^* \cdot L \cdot d$$

and will become $1.8 \cdot 10^{-3} \text{ mm}$ in this case.

Calculating the contact angle tolerances for the FA 1 and FA 2 models of the push pawls of the friction amplifying mechanism

With the relation between the contact angle α and the required minimum friction coefficient μ as

$$\mu = \tan \alpha$$

it can be calculated how large the tolerances for the contact angle are to get a certain friction coefficient tolerance. In table 5 the relations between these variables are shown as well as the tolerances for the required friction coefficients for the different geometries. It can be seen that for each geometry the tolerances for the contact angle α are around ± 3 degrees.

Contact angle α in [degrees]	Required minimum friction coefficient μ	Geometry 1: $\mu = 0.3 \pm 0.05$	Geometry 2: $\mu = 0.4 \pm 0.05$
15	0.26		
16	0.27		
17	0.29		
18	0.30		
19	0.32		
20	0.34		
21	0.35		
22	0.37		
23	0.38		
24	0.40		
25	0.41		
26	0.43		
27	0.44		
28	0.45		
29	0.47		
30	0.48		

Table 5: Contact angle VS required minimum friction coefficients to show angle tolerances for the different geometries.

With understanding the basic important geometry of the push pawls, the manufacturing tolerances can be found. Figure 61 shows the important geometry of a push pawl and the drum, where point A is the main shaft, point B is the shaft through the pawl and point C is the contact point of the pawl and the drum. The measured angle is the contact angle.

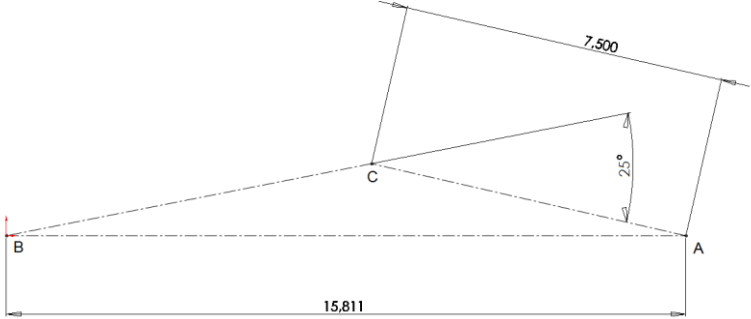


Figure 61: Sketch of the important geometry of a push pawl and the drum.

When any of the lengths AB, AC or BC changes, the contact angle will change accordingly. Measuring the changes in the SolidWorks sketch, it was found that for each length, a change of ± 0.03 mm would result in a change of the contact angle of $\pm 1.0^\circ$. Since the total change of contact angle is almost the same as the addition of all changes in contact angle due to all separate length deviations, this will be a good tolerance to ensure a total contact angle change of maximum 3° .

Appendix G: Calculations for the future design

Forces through the drum

Since the friction coefficient is quite low, the forces through the drum and the pawls will be very high. A calculation of these forces is therefore required to ensure the right choice for bearings and shafts.

The friction coefficient is found to be between 0.12 and 0.18. When choosing a contact angle α of 7° for the future design, resulting in a ratio between the normal force and friction force of 0.12.

First, the friction force has to be calculated:

$$F_f = \frac{T}{r}$$

$$F_{pawl} = \frac{F_f}{\sin \alpha}$$

$$N = F_{pawl} \cos \alpha$$

With T the locking torque of 2.0 Nm, r the radius of the drum, F_f the friction force, F_{pawl} the force through the bar and N the normal force through the drum.

With several drum radii, the following forces are found:

r	F_f	F_{pawl}	N
7.5 mm	270 N	2.2 kN	2.2 kN
10 mm	200 N	1.6 kN	1.6 kN
15 mm	130 N	1.1 kN	1.1 kN

Maximum shear stresses and safety factor for pawl shafts

Depending on the radius of the drum, the shear force on the shafts will vary. Since the main shaft has a larger radius than the pawl shafts, only the latter ones have to be reviewed.

Using a drum radius of 10 mm, the maximum force through the friction pawls will be 1.6 kN. Since the pawl shafts are connected to the phalange at both sides, the maximum force at a shaft F_{shaft} will not exceed half this force, so 800 N.

Choosing a shaft with a radius of 2 mm, this gives a cross-sectional area A of 12.6 mm^2 .

The maximum shear stress τ_{max} can be calculated as:

$$\tau_{max} = \frac{4F_{shaft}}{3A} = \frac{4 \cdot 800}{3 \cdot 12.6} = 85 \text{ MPa}$$

The yield shear stress τ_y of a material is linked to the yield tension stress σ_y with a constant:

$$\tau_y = \frac{\sigma_y}{\sqrt{3}}$$

So a high strength steel with a yield stress of 800 Mpa, will result in a yield shear stress of 460 MPa. Then, the safety factor i for breaking will be:

$$i = \frac{\tau_y}{\tau_{max}} = \frac{460}{85} = 5.4$$

This means that the pawl shafts will break when a locking torque of 5.4 times the required 2.0 Nm is applied, so 10.8 Nm.

It would be favorable to have the shafts break at a lower locking torque, so the shafts could function as the overload protection mechanism. If construction steel is used with a yield stress of 500 MPa, the yield shear stress will become 290 MPa, the safety factor will be 3.2 and the locking torque when the shafts will break will be only 6.4 Nm.

References

- [1] Atkins DJ, Heard DCY, Donovan WH. Epidemiologic overview of individuals with upper-limb loss and their reported research priorities. *Journal of Prosthetics and Orthotics*. 1996;8(1):2-11.
- [2] B. Peerdeman, D. Boere, H. Witteveen, R. Huis in 't Veld, H. Hermens, S. Stramigioli, J. Rietman, P. Veltink, and S. Misra. Myoelectric forearm prostheses: State of the art from a user-centered perspective. *Journal of Rehabilitation Research & Development (JRRD)*, 48(6):719–738, July 2011.
- [3] M. Wassink, R. Carloni, S. Stramigioli. Port-Hamiltonian analysis of a novel robotic finger concept for minimal actuation variable impedance grasping, in *IEEE Int. Conf. Robot. Autom.*, May 2010.
- [4] R. Pape, D.H. Plettenburg. The effect of joint locks in underactuated hand prostheses. MSc Thesis report, Biomedical Engineering, Delft University of Technology, 2011.
- [5] J.L. Pons, E. Rocon, R. Ceres, D. Reynaerts, B. Saro, S. Levin, and W. van Moorleghem. The MANUS-HAND dextrous robotics upper limb prosthesis: Mechanical and manipulation aspects. *Autonomous Robots*, 16(2):143-163, 2004.
- [6] S. Jung, S. Kang, and I. Moon. Design of biomimetic hand prosthesis with tendon-driven five fingers. In *Biomedical Robotics and Biomechanics, 2008. BioRob 2008. 2nd IEEE RAS & EMBS International Conference on*, pages 895-900, 2008.
- [7] S.A. Dalley et al. Design of a multifunctional anthropomorphic prosthetic hand with extrinsic actuation. *IEEE/ASME Transactions on Mechatronics*, 14(6):699-706, 2009.
- [8] M.C. Carrozza, G. Cappiello, S. Micera, B.B. Edin, L. Beccai, and C. Cipriani. Design of a cybernetic hand for perception and action. *Biological Cybernetics*, 95(6):629-644, 2006.
- [9] C. Cipriani, M. Controzzi, and M. C. Carrozza. Progress towards the development of the smarhand transradial prosthesis. In *Rehabilitation Robotics, 2009. ICORR 2009. IEEE International Conference on*, pages 682-687, 2009.
- [10] Heckathorne, 1992. Cited by M. Kutz. *Standard handbook of biomedical engineering and design*. Chapter 32, page 3. McGraw-Hill, New York, 2002. ISBN: 0071449337.
- [11] MyoHand VaryPlus Speed, Otto Bock.
http://www.ottobock.com/cps/rde/xchg/ob_com_en/hs.xsl/19932.html, 2011
- [12] H. Huang, L. Jiang, Y. Liu, L. Hou, H. Cai. The mechanical design and experiments of HIT/DLR prosthetic hand. *IEE Int. Conf. on Robotics and Biomimetics*, December 2006.
- [13] F. Lotti, P. Tiezzi, G. Vassura, L. Biagiotti, C. Melchiorri, UBH 3: An anthropomorphic hand with simplified endo-skeletal structure and soft continuous fingerpads, *IEEE International Conference on Robotics and Automation, ICRA '04, New Orleans, 2004*.

- [14] B. Buchholz and T. J. Armstrong. An ellipsoidal representation of human hand anthropometry. *Human Factors: The Journal of the Human Factors and Ergonomics Society*, 33:429–441, 1991.
- [15] W.E. Morton, J.W.S. Hearle. *Physical Properties of Textile Fibres*, second ed. pp. 611, Heinemann, London, 1975.
- [16] J.H. Jung, N. Pan, T.J. Kang. Capstan equation including bending rigidity and non-linear frictional behavior. *Elsevier, Mechanism and Machine Theory* 43:661-675, 2008.
- [17] H. R. Hertz. On contact between elastic bodies. *Collected works*, Vol. 1. Leipzig, Germany, 1895.